Pr#1192

FORMAL REPORT

GERHTR-166

UNITED STATES--GERMAN HIGH TEMPERATURE REACTOR RESEARCH EXCHANGE PROGRAM

Original report number JUL-1275
Title Fracture Toughness Testing of a Reactor Grade Graphite

Author(s) M. Roding et al
Originating Installation Kernforschungsanlage Julich, Gesellschaft mit beschrankter Haftung
Date of original report issuance March 1976
Reporting period covered

Translated from the original German

This report, translated wholly or in part from the original language, has been reproduced directly from copy prepared by the United States Mission to the European Atomic Energy Community

THIS REPORT MAY BE GIVEN UNLIMITED DISTRIBUTION

ERDA Technical Information Center, Oak Ridge, Tennessee

MASTER

GERHTR - 166
Distribution Category UC-77

KFA KERNFORSCHUNGSANLAGE JÜLICH
Gesellschaft mit beschränkter Haftung

Institute for Reactor Materials

Fracture Toughness Testing of a Reactor Grade Graphite

by

M. Röding, G. Klein, H. Schiffers and H. Nickel

Jül - 1275
March 1976

Printed as manuscript

Fracture Toughness Testing of a Reactor Grade Graphite

by

M. Rödig
G. Kleist
H. Schiffers
H. Nickel

ABSTRACT

Fracture mechanics is a well established tool for the assessment of brittle fracture in metallic structural materials.

In this paper an attempt is made to apply fracture mechanics to a reactor-grade graphite. The effect of several test parameters on the stress intensity factor was measured; this was found to lie in the range 25 and 50 $N/mm^{-3/2}$. The results are discussed in terms of the well known mechanical characteristics of graphite.

Table of Contents

		Page
1.	Introduction	1
2.	Graphite	2
2.1	The Graphite Monocrystal	2
2.2	Polycrystalline Graphite	3
2.2.1	Structure and Production	3
2.2.2	Mechanical Properties	5
3.	Principles of Fracture Mechanics	7
3.1	Early Formulae for the Development of a Brittle Fracture Criterion	7
3.2	Linear-Elastic Fracture Mechanics	11
3.3	Problems of Specimen Size and Plasticity	15
3.4	Experimental Determination of the Fracture Toughness	16
4.	Literature Review	18
5.	Fundamental Problems in the Application of Fracture Mechanics to Graphite	20
6.	Experimental Procedure	22
6.1	Materials	22
6.2	Fracture Toughness Specimens	22
6.2.1	Specimen Type	22
6.2.2	Specimen Preparation	23
6.2.3	Nomenclature of the Specimens	24
6.3	Test Rig and Test Procedure	24
6.3.1	The Testing Machine	24
6.3.2	Determination of the Critical Parameters	25
6.3.3	Electrical Potential Measurement	27
6.3.4	Definition of the Critical Stress Intensity Factors K_{Iv} and K_{Imax}	28
6.3.5	The Incipient Crack	28

		Page
6.4	Apparatus for the Microscopic Study of Crack Propagation	29
7.	Results and Discussion	30
7.1	The Fracture Behavior of Graphite	30
7.2	Influence of Various Parameters on the Fracture Toughness of Graphite	33
7.2.1	Influence of the Test Movement Rate	33
7.2.2	Influence of the Crack Length	35
7.2.3	Influence of Specimen Size	38
7.2.4	Influence of Prestressing	41
7.2.5	Influence of the Electrode and Place from which the Specimen is obtained	45
7.2.6	Influence of the Grain Size	46
7.3	The Critical Load	47
8.	Summary and Conclusions	48

Annex

References

1. Introduction

High-energy, free neutrons with mean energies of about 2.5 MeV are produced in the reactor during nuclear fission. To maintain a chain reaction, a sufficiently large number of neutrons have again to be supplied to the fuel. This is achieved by surrounding the reactor core with a reflector.

Uranium has the highest capture cross-section for thermal neutrons ($\approx$0.05 eV). For this reason it is necessary to slow down (to "moderate") the fast neutrons to thermal energies. The most suitable moderators are materials with a low atomic weight. A further requirement for moderator materials is that they themselves should absorb only a very small proportion of the neutrons, i.e., they should have a low neutron capture cross-section.

Light water, heavy water, beryllium and carbon (in the form of graphite) are generally envisaged as moderator materials on the basis of these criteria. The most suitable material is heavy water, which is however rarely used as a result of its high production costs. Graphite is very much less expensive and is therefore preferred in spite of its less satisfactory moderating properties. An essential condition in this case, however, is that it should have a low degree of contamination by substances which absorb neutrons (boron, rare earths).

Apart from the above advantages, the solid physical state and the good processing capacity are arguments in favor of the use of graphite as a moderator and reflector material. Finally, its thermal properties appear particularly suitable for use in the high-

temperature reactor. There is no reduction in its strength with an increases in temperature, the thermal expansion is low and the thermal conductivity good.

Graphite is used in the reactor as a structural material for fuel elements and reflector blocks. During operation it is subject to variable mechanical stresses due to temperature and neutron flux gradients. The general practice up to now has been to use the tensile strength in the uniaxial tensile test for the safety evaluation. To supplement this, it will now be examined what advantages the method of fracture mechanics analysis has to offer for the safety evaluation.

In the present paper unirradiated graphite specimens will undergo fracture toughness testing. The results will be given as a function of various test parameters and discussed in relation to the physical properties of the material.

2. Graphite (Ref. 1)

2.1 The Graphite Monocrystal

Apart from diamonds, carbon consists in the solid physical state of hexagonal arrangements of atoms in lattice planes. These planes may assume a wide variety of positions in relation to each other. The highest degree of order is reached in the graphite lattice in which the layer planes are parallel to each other and assume the position shown in Fig. 1. The continuous lines represent in this case the uppermost layer and the interrupted lines the second layer. The third layer is again located directly under the first.

Within the lattice planes each atom is permanently bound to its three nearest neighbors. The bond between the lattice planes is not a strong one.

The layered structure results in a number of properties being direction-dependent. Table 1 shows a number of selected physical parameters of the graphite monocrystal parallel (") and perpendicular ($\perp$) to the layer planes.

2.2 Polycrystalline Graphite

2.2.1 Structure and Production

Polycrystalline graphite consists of two principal components, the coke or natural graphite filler grains and a carbon-containing binder which insures cohesion. The graphitization process, during which the material is heated to temperatures of 2500-3000°C, insures the growth of the hexagonal carbon planes and their ordered arrangement in graphite crystallites. Defective compression during the pressing process and the escape of pyrolysis gases during heating give rise to so-called macropores between the grains. "Micropores" inside the coke grains are produced by the ordering function of the graphitization process and the consequent material compression and also by stress cracks which occur during cooling from the graphitization temperature. Fig. 2 shows in diagrammatic form a cross-section through a graphite grain.

The anisotropy of the graphite monocrystal affects also the shape of the filler grains, which are generally oblong. As a result of structure formation during the compression process, the anisotropic behavior is carried over to the physical properties of the macroscopic graphite body. Some of the principal data are summarized in Table 2 in order to give an idea of these properties. The material is graphite AS2-F-500 which was the subject of the present study. Further information on this graphite is given in Section 6.1.

The manufacturing process for an industrial

graphite is shown in Fig. 3 in the form of a flowsheet. This will be explained below.

Materials of different origin are used as filler grains. The most suitable for pre-graphitization are natural graphite grains, their disadvantage being the high anisotropy of the macroscopic graphite body. Isotropic graphites are obtained with isometric gilsonite grains, which are however only seldom used for graphite production in view of the small raw material reserves (only one mine). Oil coke, obtained as a byproduct of mineral oil processing, is more suitable for graphitization than pitch coke obtained from coal-tar pitch; nevertheless pitch cokes are predominantly used in West Germany as a result of their low price and good availability.

The raw cokes still contain large fractions of volatile hydrocarbons. The material is heated to 1200-1400°C in a so-called calcination process, in order to expel the volatile components. The material is then subjected to grinding and fractionation. The grain fractions are mixed in the desired quantity ratios and the binder added to them. Synthetic resins and coal-tar pitches are used as binders. The criteria for the choice of binder are good graphitization qualities and a high carbon yield.

The so-called green mass is compressed into moulds. Extrusion is the most widely used process, but die-stamped graphite is also produced. A broadly isotropic graphite is obtained with isostatic compression, in which the pressure is applied to the material uniformly by means of a liquid.

The green moulds at present available easily

lose their shape as a result of the softening of the binder with an increase in the temperature. Careful coating of the binder is therefore carried out at 800-1000°C. It is important in this case to provide support for the material, in order to prevent alteration of the shape. The burnt material, the so-called hard burnt coal, acquires during combustion a pore fraction in excess of 25 % due to the process of shrinkage. An impregnation agent (generally coal-tar pitch) is pressed into the pores to increase the density.

The graphitization process, which constitutes the final stage, requires about two weeks, the greater part of which is taken up with cooling. Cooling has to be carried out slowly in order to keep the thermal stresses at a low level and to prevent as far as possible crack formation.

2.2.2 Mechanical Properties

The behavior of graphite under external stresses can be most simply described on the basis of the stress-strain characteristic curve (Fig. 4). Graphite differs from most other materials in having no detectable proportional range, i.e., the curve follows a curved pattern virtually from its point of origin (Ref. 4). Unless exposed to excessively high loads, the curves can be described by the following approximation formula given by Jenkins (Ref. 5) :

$$\varepsilon = A\,\sigma + B\,\sigma^2 \qquad (1)$$

in which ε = strain
σ = stress
A = reciprocal of the modulus of elasticity at the point of origin
B = constant.

The constants A and B are functions of the test velocity and the temperature.

When exposed to any stress σ_o with a corresponding strain ε_o below the fracture point, followed by relaxation, the specimen retains a residual strain ε_1. Depending on the material, direction of the cross-section and test velocity, the amount of this strain will be $\varepsilon_1 = 0.1\ \varepsilon_o$ to $0.3\ \varepsilon_o$. With renewal of the stress the curve again follows the pattern given by formula (1) from the point $(\sigma_o, \varepsilon_o)$ onwards. On reaching the breaking stress the specimen fails suddenly, without undergoing appreciable deformation on the fracture surfaces. The elongation at fracture is < 0.5 %.

The behavior described is typical both of tensile and also compression stresses. The determination of a modulus of elasticity or of deformation

$$E = \frac{d\sigma}{d\varepsilon} \qquad (2)$$

involves considerable difficulties in graphite. It depends on the stress applied and the previous history of the specimen. For comparison purposes the reference elastic modulus can be defined as the slope of a secant through a fixed point on the curve. A more usual procedure is to give the dynamic elastic modulus which can be determined by means of acoustic velocity measurements in the material (Ref. 6). This modulus is virtually identical with the slope of the stress-strain curve at the point of origin.

Graphite undergoes substantial structural and geometrical changes in the high-temperature reactor. A distinction has to be made, however between the different areas in the material. In areas of poor graphitization a radiation-induced regraphitization occurs, causing a shrinkage of the material as a result of

the ordering effect. In the crystalline region, defects are produced as a result of the bombardment with fast neutrons, predominantly in the form of Frenkel defects. The diffusion of a large number of voids on the surface causes shrinkage of the crystallites in directions parallel to the lattice planes. Frequent aggregations of interlattice atoms to form clusters result in an expansion perpendicular to the lattice planes.

Changes in the physical properties, on occasion substantial, occur under reactor conditions as a result of the structural changes in the graphite. The curves of these properties as a function of the dose are in general highly complex and cannot be described in a few words. They depend on a whole number of parameters (irradiation temperature, graphitization temperature, material composition, etc.).

3. Principles of Fracture Mechanics (Refs. 7-9)

3.1 Early Formulae for the Development of a Brittle Fracture Criterion

It has long been known that fractures in materials originate from faults and cracks. Only in 1913, however, was a first attempt to describe this problem made by Inglis (Ref. 10). This author calculated the increase in the stress at the end of an elliptical hole in an infinitely long plate under an external stress σ_o (Fig. 5) in the following form :

$$\sigma_{max} = \sigma_o(1 + 2\frac{a}{b}) \qquad (3)$$

in which a : large semiaxis of the ellipse
b : small semiaxis of the ellipse

If a fine internal crack in the plate ($a/b \to \infty$) is present in place of the elliptical hole, the equation gives the stress $\sigma_{max} = \infty$.

This only applies, however, to homogeneous materials having an ideal elasticity. In real materials the high stresses at the crack front are always eliminated by local plastic effects. The considerable increase in the stress at the tip of the crack indicates that here for the first time the atomic tensile stress, i.e., the stress required to separate two atom layers, has been exceeded. A fracture will therefore always start from here.

A first fracture criterion for brittle materials was published by Griffith in 1920 (Ref. 11). He established the energy balance for a plate into which a crack of length 2a had been introduced.

For the crack to develop work has to be done against the cohesive forces of the molecules. This work appears in the energy balance as consumed surface energy. If the crack is sufficiently large, so that the crack sides are more widely separated than the radius of the molecular interaction at all points except in the immediate vicinity of the tip, the surface energy U_S, generated by the crack, is proportional to the resulting surface :

$$U_S = 4\ a d \alpha \qquad (4)$$

in which a : crack length
d : plate thickness
α : specific surface energy.

Using the Inglis formula Friffith calculated that the loss of elastic energy U_e occurring as a result of the introduction of the crack would be

$$U_e = - \frac{\pi a^2 \sigma^2 d}{E} \qquad (5)$$

Disregarding the plastic energy fractions,

the variation in the potential energy during the occurrence of the crack is

$$\Delta U = U_e + U_S = 4ad\alpha - \frac{\pi a^2 \sigma^2 d}{E} \qquad (6)$$

A steady-state for the energy in relation to a is reached when

$$\frac{\partial (U_e + U_S)}{\partial a} = 0, \qquad (7)$$

or

$$a \sigma^2 = \frac{2 \alpha E}{\pi} \qquad (8)$$

A crack will only be propagated spontaneously, i.e., without the application of further energy from the outside, if condition (8) is fulfilled. This provides, therefore, a fracture criterion for structures which are subject to cracks : A critical stress σ_c can be applied to a given crack length 2a, which leads to an unstable fracture

$$\sigma_c = \sqrt{\frac{2 \alpha E}{a \pi}} \qquad (9)$$

On the other hand, it is possible to indicate for a plate, which is exposed to a fixed external stress, a critical crack length

$$2a_c = \frac{4 \alpha E}{\sigma^2 \pi} \qquad (10)$$

at which it will fail. This crack length 2a is known also as the Griffith length.

Equation (8) is only valid for the two-dimensional stress state. In the two-dimensional strain

state*) it becomes :

$$a\,\sigma^2 = \frac{2\,E\,\alpha}{\pi(1-\nu^2)} \qquad (11)$$

in which ν: Poisson constant

Suitable corrections have to be applied to equations (9) and (10) for the two-dimensional strain state.

A graph presentation of the energy condition as a function of the crack length is shown in Fig. 6. It is clear that energy will have to be supplied from outside, if the crack is to increase to the length $2a_c$. After this point the surface energy consumed can be satisfied from the elastic energy released alone.

Experimental verifications of the theory in relation to glass materials (Ref. 12) revealed inadequate agreement. The reason for this is the low plastic deformation phenomena occurring at the tip of the crack, which are always present also in macroscopically brittle materials like glass and which are not covered in the Griffith formula. In addition to the surface energy consumed,

---

*) In a finitely thick plate, which is under external load, the stress distribution in the neighborhood of the surface is influenced by transverse contraction. A variation occurs at that point in the stress conditions over the thickness of the specimen. If the specimen is sufficiently thick, the transverse expansion of the internal material will be prevented by the external regions, so that the stress conditions no longer vary over the complete thickness of the specimen. In the first case we speak of the two-dimensional stress state and in the second case of the two-dimensional strain state.

a term for the plastic energy consumed γ had to be included in equation (8), which then became

$$a\,\sigma^2 = \frac{1}{\pi}\,2E\,(\alpha + \gamma) \qquad (12)$$

This form of the Griffith condition is of no practical importance, since the quantitative determination of γ is in general difficult.

3.2 Linear-Elastic Fracture Mechanics

A more general interpretation of the fracture process was introduced by Irwin (Refs. 13 and 14). The basic features of his theory will be briefly outlined here.

If any stress is applied to a plate which is subject to cracks, any number of kinds of stress can in principle occur at the tip of the crack, which can, however, be represented by superimposition of three basic modes of crack opening (Fig. 7).

The stress distribution in the neighborhood of the tip of the crack was calculated by Sneddon (Ref. 16) for an infinitely extensive plate of thickness "1", using the Westergaard stress function (Ref. 17). The general result for any stress modes (we shall consider subsequently only the right-hand tip of the crack - Fig. 8) runs as follows :

$$\sigma_{ik} = \frac{K_n}{\sqrt{2\pi r}}\,F^n_{ik}(\varphi) \qquad (13)$$

in which i,k : x, y, z
n : I, II, III

$F^n_{ik}(\varphi)$ is in this case a purely angular function. K_n is initially only a constant, dependent only on the external load and the

specimen geometry; it is known as the stress intensity factor and has the dimension N $mm^{-3/2}$.

In the special case of the stress according to mode I, we obtain from (13) :

$$\sigma_x = \frac{K_I}{\sqrt{2\pi r}} \cos\frac{\varphi}{2}\left(1-\sin\frac{\varphi}{2}\sin 3\frac{\varphi}{2}\right)$$

$$\sigma_y = \frac{K_I}{\sqrt{2\pi r}} \cos\frac{\varphi}{2}\left(1+\sin\frac{\varphi}{2}\sin 3\frac{\varphi}{2}\right) \qquad (14)$$

$$\tau_{xy} = \frac{K_I}{\sqrt{2\pi r}} \sin\frac{\varphi}{2}\cos\frac{\varphi}{2}\cos 3\frac{\varphi}{2}$$

Examining the stress curve in the plane y = 0 alone, we obtain

$$\sigma_x = \sigma_y = \frac{K_I}{\sqrt{2\pi r}} \qquad *) \qquad (15)$$

$$\tau_{xy} = 0$$

The stress intensity factor can therefore be regarded as a criterion for the excessive increase in the stress at the tip of the crack (cf. Fig. 9) :

$$K_I = \lim_{r \to 0} \sigma_{(x)} \sqrt{2\pi r} \qquad (16)$$

The stressing of a plate, the width b of which is large in relation to the crack length a, is governed by the mode I stress

$$K_I = \sigma \sqrt{\pi a}; \qquad (17)$$

---

*) Equations (13) to (15) were calculated on the assumption that $r \ll a$; they apply only in the immediate vicinity of the tip of the crack. At greater distances σ_x goes to zero and σ_y in the direction of the external stress σ.

In the case of a finite plate width b, the equation has to be corrected by a geometry factor f(a/b). The formula then runs :

$$K_I = \sigma \sqrt{\pi a f(a/b)} \qquad (18)$$

The particular importance of the stress intensity factors K is that they provide information on the critical values K_c, on reaching which the specimen fails. These K_c values are no longer a function of the geometry of the specimen, but of the material alone. A wide variety of tests on various materials have shown that the material-specific values K_c can be used as a failure criterion for brittle fracture.

The smallest K_c values occur with the stress mode I (Ref. 15), so that in practice the parameter K_{Ic} is used for evaluation of the fracture behavior. The critical stress intensity factor K_{Ic} is designated the fracture toughness.

K_{Ic} can be determined directly from equation (17) or (18). It is merely necessary, in the case of stressing according to mode I, to measure the critical parameters, crack length and external stress, at the moment of failure.

Irwin also carried out in Ref. 14 an energy analysis of the fracture process. He again based his analysis in this case on the infinitely large plate with an internal crack of length 2a. Where exposed to an external stress, the material undergoes predominantly elastic stressing, i.e., plastic deformations are possible only in the neighborhood of the tip of the crack. The plastic range will in this case be small in relation to the

crack length. If a widening of the crack occurs, the expansion energy U, stored in the plate, is decreased by :

(a) the fraction which is attributable to non-reversible displacement of the points of application of the force (and which is disregarded here),

(b) the loss of elastic energy caused by the widening of the crack.

The latter fraction is designated G. In the linear-elastic case for a plate of thickness "1"

$$\frac{dU}{2da} = G \qquad (19)$$

G has the dimension of a force and has been designated by Irwin the crack extension force. He regards it as the force which is attempting to draw a crack further into the specimen. If the crack extension force exceeds a critical value G_c, propagation of the crack occurs.

In the case of the G values also, the nature of the crack opening has to be differentiated accordingly into G_I, G_{II} and G_{III} (Fig. 7). The stress intensity factor K_I and the crack extension force G_I are connected for the two-dimensional stress state by the formula

$$K_I = \sqrt{G_I \cdot E} \qquad (20)$$

and for the two-dimensional strain state

$$K_I = \sqrt{\frac{G_I \cdot E}{1-\nu^2}} \qquad (21)$$

in which E is the elasticity modulus.

As a measuring technique for the determination

of G or G_{Ic}, Irwin introduced in Ref. 13 the formula

$$G_I = \frac{1}{2} P^2 \frac{d}{da} \left(\frac{1}{M}\right) \qquad (22)$$

in which P is the load applied and M the spring constant of the specimen. The function $\frac{d}{da} \left(\frac{1}{M}\right)$ depends on the crack length and can be determined by measuring M at various crack lengths.

This so-called compliance method (the parameter 1/M is designated compliance in English) can also be used to determine the correction function f(a/b) in equation (18) for any desired specimen shape. The connection between equations (22) and (18) is provided in this case by equation (20) or (21).

3.3 Problems of Specimen Size and Plasticity

Linear elastic fracture mechanics apply strictly only to specimens which are subject to a purely elastic stress. This condition is not met in real materials. If, however, the range of plastic deformation phenomena is small in relation to the specimen dimensions, it may be disregarded and the calculation carried out on a linear-elastic basis. The approximate dimensions and shape of the plastic range at the tip of the crack can be calculated (Ref. 15). For this purpose the main stresses are determined from equation (14) and the reference stress calculated therefrom in accordance with the shape alteration hypothesis

$$\sigma_v = \frac{1}{\sqrt{2}} \left(\sigma_1 - \sigma_2 \right)^2 + \left(\sigma_2 - \sigma_3 \right)^2 + \left(\sigma_3 - \sigma_1 \right)^2 \qquad (23)$$

The plastic zone is limited then by the surface area on which this reference stress is equal to the yield stress σ_F. The shape of the plastic zone is shown in Fig. 10 and its order of magnitude can be estimated from

$$r_F = \frac{1}{2\pi} \left(\frac{K_{Ic}}{\sigma_F}\right)^2 \qquad (24)$$

in which r_F is the "radius" of the plastic zone and σ_F is the yield stress in the uniaxial tensile test.

If the specimen dimensions have the order of magnitude r_F, the condition that the propagation of the crack is predominantly controlled by a linear-elastic stress-strain field no longer holds good. The influence of plastic deformation phenomena yields in this case too high values in the determination of K_{Ic}. It is therefore important to keep to minimum dimensions in the determination of the fracture toughness values. These minimum specimen dimensions are in general given as a multiple of r_F.

The first attempt to incorporate the plastic deformation phenomena at the tip of the crack in equation (18) was made by Dugdale (Ref. 18). He attempted to compensate for the plastic effects by a theoretical crack length

$$c = a + r_F \qquad (25)$$

The stress intensity factor is found in this case to be

$$K_I = \sigma \sqrt{c\ \pi\ f(c/b)}. \qquad (26)$$

The difficulty with this model lies in the determination of the exact value of r_F. Furthermore, r_F is not a true constant, but has a value dependent rather on the previous strain history, the temperature and the load velocity.

3.4 Experimental Determination of the Fracture Toughness

In recent years the science of rupture mechanics

has acquired great importance in the assessment of the strength of metal components. Methods of measurement have been standardized and in the USA there is today even an ASTM standard regulation for the K_{Ic} determinations on metal materials (Ref. 19).

The correction function f(a/b) in equation (18) can be determined mathematically for various types of specimen. Since it is independent of the elastic properties of the material, recourse may be had to the data in the literature. A review of the literature relating to more than 140 specimen shapes is given in Ref. 20.

The specimens most frequently used are of the unilaterally notched tensile and bending type. In the ASTM standard regulation the unilaterally notched three-point bending specimen and the CT specimen (see Section 6.2.1) are permitted.

If in the fracture toughness tests the load P is plotted against the crack opening o the ideal curve pattern in Fig. 11a is not always obtained; curves such as those in Figs. 11b or 11c are more common. The most common reason for this is that the plate thickness is on the boundary of the permissible value. These curves can, however, still be used for evaluation, since even with thin specimens the two-dimensional strain state applies in the center and extension of the crack starts on reaching K_{Ic}. The crack is however halted as a result of the two-dimensional stress state in the vicinity of the surface and the consequent greater plastic deformation.

When the crack extension enters the center

of the specimen, a "pop-in" frequently appears in the load-expansion curve (Fig. 11b). The corresponding load can be used for determination of K_{Ic}. Since, however, the pop-in does not always emerge clearly, the 5 % secant method was proposed by Brown and Srawley (Ref. 21), and has also found acceptance in the ASTM regulation. According to this method any load may be regarded as critical, which is obtained from the point of intersection of the load-expansion curve and the secant which has a slope 5 % less than the slope of the original tangent (Fig. 11c).

Other methods, which react sensitively to crack extension, have also been used for determination of the critical load. The variation of the electrical resistance over the specimen cross-section (Ref. 22) or ultrasonic emission (Ref. 23) are frequently used as indicators.

It follows from equation (3) that the danger of a crack increases with the sharpness of the tip of the crack. In order to obtain a valid K_{Ic} value, i.e., a value which covers also even unfavorable conditions, the crack introduced in the specimen should be as fine as possible. The general practice with metals is to introduce a fine fatigue crack into the metal from the tip of a saw section. This is done by a repeated alternating stress at a low load amplitude.

4. Literature Review

During fracture toughness studies on various ceramic materials a number of authors have tested also individual graphite specimens. Several more far-reaching papers have also

been published in recent years on the influence of various parameters on the measured K_{Ic} and G_{Ic} values of graphite. The contents of these papers will be briefly outlined below.

The first G_{Ic} values were obtained by Corum (Ref. 24) in 1966 on four-point bending specimens. Both the compliance method in accordance with equation (22) and the analytical method in accordance with equation (18), incorporating a theoretically determined correction function, were used for evaluation of the results. The agreement between the methods was good. Corum was unable to find any dependence of the G_{Ic} values on crack length. Corum's work was confirmed by Davidge and Tappin (Ref. 25). Slind (Ref. 26) used the so-called DCB specimen (Ref. 27) for the determination of K_{Ic} and G_{Ic} values for various specimen thicknesses and crack lengths. He was unable to find that these parameters exercised any influence on the measurements.

The most comprehensive program of research on the studied parameters is that of Yahr and Valachovic (Ref. 28). These authors carried out four-point bending tests on graphites of ultrafine granularity (grain size < 100 µm). No effect of the specimen width, crack length or crack sharpness was found, but higher K_{Ic} values were found on large specimens than on small. Comparison with fracture toughness values, obtained on other types of specimen, revealed satisfactory agreement.

Brocklehurst and Brown (Ref. 29) used three-point bending specimens of an isotropic graphite. The variation in the K_{Ic} values with the crack length was very slight and

an influence of the notch width N was only found for $N < 0.6$ mm. A comparison of various specimen types revealed values which were equivalent only in terms of order of magnitude.

In addition to the papers referred to above, studies are also extant on special problems, such as the temperature dependence of the K_{Ic} value (Ref. 30) and stable crack growth (Ref. 31).

A common feature of all this work is that small numbers of specimens were examined and the statistical scattering was considerable. The results cannot therefore always be regarded as immediately reliable. A further disadvantage is that the majority of authors confine themselves to a purely formal application of fracture mechanics to the graphite without taking into account the properties specific to the material.

5. Fundamental Problems in the Application of Fracture Mechanics to Graphite

The science of fracture mechanics, as described in Section 3, applies strictly speaking only to homogeneous and isotropic materials, which in addition are exposed only to predominantly linear-elastic stresses. Graphite is neither homogeneous nor isotropic and the formation of predominantly linear-elastic stresses is difficult, if not impossible to induce.

It has already been pointed out in paragraph 2.2.2 that graphite has no detectable proportional range - an indication that the threshold stress for irreversible processes is extremely low. This means, however, that these processes can occur in a large volumetric region of the specimen which is under stress.

Residual strain down to 0.5 N/mm^2 can be detected with the apparatus available at

the IRW. This value, however, by no means represents a threshold stress for irreversible processes in graphite, but rather the strain which can just be reliably detected with the available equipment. The real yield stress will therefore undoubtedly lie below this value. Even with 0.5 N/mm^2, however, we can calculate from equation (24) on the assumption of $K_{Ic} = 35\ N/mm^{-3/2}$ a value for the radius of the "plastic" zone $r_F \approx 0.8$ m. This would require, according to ASTM regulations (Ref. 19), specimen dimensions of a few meters, which would not be experimentally verifiable. It is therefore questionable whether such a method can provide fracture toughness values independent of the specimen size. The physical causes of irreversible processes in graphite are in fact quite different from those occurring in metals (see Section 7.1).

The fracture behavior in graphite could be described by a modified Griffith criterion as in equation (12), but this cannot be applied in practice in view of the poor detectability of the "plastic" energies. The Dugdale model is again unsuitable for use in graphite, since this model detects only locally occurring plastic deformations.

In view of the anisotropic structure of graphite the strength properties are direction-dependent. In die-stamped material two and in extruded material three (see Fig. 14) directions of orientation are present. Separate fracture toughness values have to be determined for these principal directions, from which the values for other directions can be calculated.

Further difficulties arise as a result of the proneness of the material to cracking.

Since excess stresses can build up in graphite under load at each individual natural crack, marked interference occurs with the stress field of the macroscopic crack. This effect could well, however, be impossible to detect.

In spite of these difficulties the attempt has been made to determine the fracture toughness values of graphite and to obtain from the results obtained an understanding of the properties typical of the material.

6. Experimental Procedure

6.1 Materials

AS 2-500 graphite supplied by the firm SIGRI is an extruded pitch coke graphite. A distinction is made between three types based on the grain size :

AS2-G-500 : not exceeding 10 mm
AS2-M-500 : not exceeding 3 mm
AS2-F-500 : not exceeding 1 mm

This paper will deal mainly with the F material, K_{Ic} values for M and G materials being introduced only in paragraph 7.2.6 for comparison purposes.

The principal mechanical characteristics of the three graphite varieties are compared in Table 3. Further properties of the F variant will be found in Table 2.

The AS2-F-500 material used for specimen preparation was obtained from four different electrodes, which were designated electrodes I to IV for purposes of differentiation.

6.2 Fracture Toughness Specimens

6.2.1 Specimen Type

For the fracture toughness determination in graphite use was made of the so-called CT (compact tension) specimen in accordance with the ASTM proposals (Ref. 19) (see Fig. 12). The particular advantages of this specimen shape are

its low material requirement (volume ratio by comparison with the bending specimen 1 : 3.3) and its suitability for the study of subcritical crack growth and directional effects (Ref. 9).

The stress intensity factor for the CT specimen is determined (see Fig. 12) in accordance with the formula

$$K_I = \frac{P.\sqrt{a}}{b.d}\left[29{,}6 - 185{,}5\left(\frac{a}{b}\right) + 655{,}7\left(\frac{a}{b}\right)^2 - 1o17\left(\frac{a}{b}\right)^3 + 638\left(\frac{a}{b}\right)^4\right] \qquad (27)$$

This formula is valid within the range $0.3 \leq a/b \leq 0.7$. A compliance calibration of the correction function has been carried out from the load-expansion curves in paragraph 7.2.2. Satisfactory agreement was obtained.

6.2.2 Specimen Preparation

The point has already been made in Section 5 that the minimum dimensions required by the ASTM cannot be complied with in the case of graphite and that this would not in any case be necessarily desirable. To permit a determination of the variation in the fracture toughness figures with specimen size, three types of specimen were arbitrarily selected, while retaining the proportionality values proposed by the ASTM (Table 4). It was borne in mind in this case, however, that the specimen dimensions were large in relation to the grain sizes. The production tolerances were 0.01 b for b_1 and d and 0.005 b for all other dimensions.

The way in which the specimens were taken is of importance in view of the anisotropy of the material. Specimens were taken in three main directions in the case of the extruded material (Fig. 14). In the X scheme the direction of compression was perpendicular

to the fracture surface and in the Y and Z schemes parallel to it. The direction of compression in the Y scheme was perpendicular to the direction of crack propagation and in the Z scheme parallel to it.

We used in the present paper in the first place specimens obtained on the basis of scheme Z.

6.2.3 Nomenclature of the Specimens

The specimens were designated type Z 10, Z 30 or Z 60 according to their thickness (column 1 in Table 4). The letter Z represents in this case the method whereby the specimen was obtained according to Fig. 14. The type designation is followed by the serial number.

Example : Z 30-46 denotes : Specimen scheme Z
specimen thickness d = 30 mm
specimen No. 46 of type Z 30

6.3 Test Rig and Test Procedure

6.3.1 The Testing Machine

The Zwick 1385 model was available as a material testing machine (Fig. 15). The claws used for suspension of the specimens were constructed in accordance with the ASTM regulation (Fig. 16).

The load P was recorded on the machine recorder, plotted against the crack opening δ (Fig. 18a). The load was not in this case applied in proportion to the passage of time, as required by the ASTM regulation for metals. Tests with a linear increase in the load proved unsuccessful, since the machine could no longer be regulated sufficiently rapidly in the vicinity of the maximum load as a result of the small slope of the stress-strain curve. The tests were therefore

run, as in normal with ceramic materials, at a constant transverse main velocity. This corresponds also to the type of stress occurring in the reactor.

The crack opening was measured with the Hottinger DD 1 crack expansion sensor. The blades for suspension of the sensor were screwed into the front face of the specimen.

To permit the start of propagation of the crack to be followed under the microscope, a mechanical stage complete with microscope was set up on either side of the machine. This could be adjusted by means of micrometer screws. The use of cross-graticule eyepieces enabled the crack lengths, required in paragraph 7.2.4, to be measured after propagation of the crack had been induced in the machine.

6.3.2 Determination of the Critical Parameters

It was observed under the microscope in preliminary tests on graphite fracture toughness specimens that propagation of the crack began even at about 70-90 % of the maximum load. A "pop-in" seldom occurred, coinciding at the earliest with the point of observed propagation of the crack and occurring in most cases only under higher load.

The question now arose of what load was to be regarded as critical in the sense of fracture mechanics. A "pop-in" would possibly have provided a suitable criterion, had it occurred regularly. Since it did not, some other means had to be found for determining the critical load. The use of the 5 % secant method according to ASTM is not suitable for graphite. In metals

there is a physical connection between this secant and the propagation of the crack, but such a physically valid connection does not apply in the case of graphite.

The attempt was therefore made to determine the load at which propagation of the crack occurrs. This was done in the first place by observation under the microscope. The electrical potential method (see paragraph 6.3.3) was found to be more suitable, since it was free of subjective observation errors. The question of whether the start of propagation of the crack is to be regarded as critical in the sense of fracture mechanics or whether critical conditions only apply at the peak of the load-expansion curve is considered in Section 7.3. Since this question has not yet been finally clarified, in the present paper the critical stress intensity factors have been determined both from the load P_v at the start of propagation of the crack and also from the maximum load P_{max}.

Determination of the fracture toughness from P_{max} necessitates strictly speaking the use in equation (27) of the crack length a obtaining at the moment of maximum load. Determination of this parameter, however, involves considerable difficulties. The introduction of a microscope with a cross-graticule is an inaccurate procedure, since it is often difficult to determine the tip of the crack with the required speed in view of the inhomogeneous material structure. Chemical crack detection agents also fail to reveal the crack more clearly; they also appear to exercise a corrosive effect on

graphite. Measurement of the crack length with the electrical potential method (Ref. 32) is again unsuitable in view of the inhomogeneities. Since it proved impossible to develop a suitable method of crack measurement during the test, we used in equation (27) the crack length (or notch length) present at the start of the test. Although the stress intensity factors thus determined were certainly rather too low, the error was on the safe side.

6.3.3 Electrical Potential Measurement

The test rig for determination of the propagation of the crack by the potential method is shown in Fig. 17a and the corresponding equivalent circuit diagram in Fig. 17b. R_1 represents in this case the resistance of the specimen in the area of the crack and R_2 the resistance of the remainder of the specimen. As the crack advances, the specimen cross-section is reduced, R_1 becomes greater and the voltage at the measuring amplifier input rises.

If the crack opening δ is plotted against the output voltage U of the amplifier, the curve shown in Fig. 18b is obtained. The propagation of the crack, observed under the microscope, coincides with the clearly perceptible starting point of an increased voltage drop over the specimen (see Fig. 18b, arrow). Using the corresponding expansion δ, we can obtain from the load-expansion curve (Fig. 18a) the load P_v corresponding to the propagation of the crack.

An Al_2O_3 tube with a steel core was used as a bolt on the suspension (see Fig. 16), to insure

insulation of the specimens against the exposed metal parts of the machine. In view of the high elastic modulus of Al_2O_3 ($E = 3.58 \times 10^{11}$ N/m^2) by comparison with that of steel ($E = 2.1 \times 10^{11}$ N/m^2) and graphite ($E \approx 10^{10}$ N/m^2) this had no adverse effect on the application of the force. The specimens were laterally insulated against the claws by means of PVC rings.

6.3.4 Definition of the Critical Stress Intensity Factors K_{Iv} and K_{Imax}

The critical loads, determined by the electrical potential method described in paragraph 6.3.3, are designated in the present paper P_v and the corresponding fracture toughness values K_{Iv}. The maximum load of the load-expansion curve will be designated P_{max} and the corresponding critical stress intensity factor K_{Imax}.

6.3.5 The Incipient Crack

It has already been pointed out in paragraph 3.4 that artificially induced cracks in the specimen should be as fine as possible. No machine capable of producing a fatigue incipient crack was available and it is also questionable whether a fatigue crack can in fact be produced in graphite at all. As Marshall and Priddle found in cyclization tests on graphite (Ref. 33), propagation of the crack occurs in fact with variations of $\Delta K \approx 0.6\ K_{Ic}$ in the stress intensity. A variation in the mechanical behavior of a graphite specimen would in this case have occurred as a result of the preliminary stress, so that some effect on the K_{Ic} value would be expected. For the same reason again a

single preliminary stress extending to the point of propagation of the crack is not suitable (see paragraph 7.2.4). This procedure, like the production of an incipient crack with a chisel (Ref. 28), will again increase the critical stress intensity factors.

Brocklehurst and Brown (Ref. 29), working on a graphite of comparable grain size to that of AS2-F-500, replaced the fine cracks by sawn cuts. A study was made of the influence of the width of the cut N on the measured fracture toughness values. Only in the case of $N < 0.6$ mm was any influence detected. In similar studies on AS2-M-500, Buresch (Ref. 34) found an effect on the critical stress intensities even for cut widths N of less than 2 mm.

In the light of these results and the difficulties referred to above, we therefore dispensed with the need to produce a fine incipient crack. In its place fine cuts were made in the specimens with a saw. A jig saw 0.3 mm in thickness was used for this purpose. The exact length of the cut was measured with a Leitz plane-table microscope. The accuracy was $\pm$ 0.3 mm.

6.4 Apparatus for the Microscopic Study of Crack Propagation

A number of specimens were prepared as shown in Fig. 19 in order to permit crack propagation studies to be carried out independently of the universal test machine and the results photographed. The specimens could be expanded and the crack extended by means of the screw device which is also shown in the figure.

The photographs in paragraph 7.1 were obtained with this arrangement.

7. Results and Discussion

7.1 The Fracture Behavior of Graphite

Graphite is generally regarded as a brittle material. This view is derived from experience of conventional tensile tests in which specimens, exposed to a stress at a constant traverse rate, failed suddenly and without macroscopic deformation after reaching the maximum load.

The fracture process, occurring in fracture mechanics compact tension specimens, presents a different picture in the case of a constant traverse rate. A sudden fracture cannot be induced here, even after the maximum load in the load-expansion curve has been exceeded.

It could be seen under the microscope that crack propagation was a discontinuous process in the case of short crack lengths, i.e., the crack advanced in each case by short distances of 1-2 mm and then stopped again. The extent of these discontinuous increases in the crack became smaller with an increase in the crack length, until finally ($a/b \approx 0.5$) the crack front moved forward in quasi-continuous fashion.

The course of the crack is subject to sharp changes of direction within a mean direction of fracture. As is evident from photographs in polarized light (Fig. 20), this is due to the fact that the crack is following the structural lines in the material. Changes of direction are also caused in general by grains which are unfavorably positioned for the crack (Fig. 21). Fracturing of the grain seldom occurred, but more frequently in the coarse-grained material AS2-M-500

than in the fine-grained material AS2-F-500 (this is apparent also from observations on the fracture surfaces). The crack can also be deflected from its original direction by large pores, however, whereas it is virtually unaffected by small pores (Fig. 22).

The fracture surfaces of a number of fractured specimens have also been studied under the scanning electron microscope, but no fresh information was obtained on the course of the fracture.

Increased stresses occur in accordance with equation (3) under external loads in the numerous natural cracks in graphite. Such stresses lead to the loosening of bonds in the material, i.e., to an increase in these fine cracks. In addition to slip processes, this enlargement and generation of cracks, extending down to microcracks in the crystallites, is the principal cause of the irreversible consumption of energy as a result of the load. If in addition a long crack is already present in the specimen, this will exercise a pronounced influence on the small cracks by means of its stress field. The consequence of this is a particularly frequent and obvious occurrence of secondary cracks in the neighborhood of the tip of the long crack (Fig. 23), since this is the zone where the highest stresses occur.

The frequent occurrence of secondary cracks in the neighborhood of the tip of the primary crack, which has been described above, and the consequent high consumption of irreversible energies provides the explanation for the halting of cracks in graphite. As the crack advances

into the interior of the specimen, it pushes in front of it a stress field which generates all the time new secondary cracks. If the energy supplied is less than the energy irreversibly consumed, the crack comes to a stop. Examined from the point of view of the energy expended, it is again clear that the advance of the crack Δa will be greater with small crack lengths a than with large crack lengths. For a specimen of thickness "1" the following energy balance applies :

$$dU = \gamma\, 2da + d\Phi \qquad (28)$$

in which dU is the amount of energy consumed to enlarge the fracture surface by dA = 1, γ is the mean specific surface energy and $d\Phi$ the irreversibly dissipated energy. The latter quantity can, disregarding the dependence of crack length on irreversible energy (cf. paragraph 7.2.2), be regarded in a first approximation as proportional to the extension of the crack

$$d\Phi = \varphi\ 2\ da \qquad (29)$$

in which φ is the specific irreversible energy consumption.

Equation (28) can then be written down in the following form :

$$\Delta U = (\gamma + \varphi)\ 2\ \Delta a \qquad (30)$$

This equation states that the extension of the crack Δa is proportional to the energy ΔU introduced into the crack.

The energy ΔU, consumed during expansion of the crack by Δa, is supplied by the elastic energies stored in the machine and in the specimens. It may be assumed in view of the low fracture loads of graphite and the high rigidity of the machine that

the energy stored outside the specimen is low in relation to the deformation energy contained in the specimen. The latter has been determined by planimetric measurement of the load-extension curve for various crack lengths a/b. A reduction in the stored deformation energy U_g was found in this case with the relative crack length a/b (Fig. 24).

Now it is certain that not all the stored energy is used for propagation of the crack (this is demonstrated by the partial elastic reversal of deformation on removal of the load after the crack has advanced). It may be assumed, however, that a reduction in the stored energy U_g will be accompanied by the expenditure of less energy ΔU for propagation of the crack. According to equation (30) this is equivalent to a reduction in the growth of the crack Δa. The curve in Fig. 24 can therefore be used to explain the reduction in the crack growth Δa with the crack length, which has been observed under the microscope.

7.2 Influence of Various Parameters on the Fracture Toughness of Graphite

7.2.1 Influence of the Test Movement Rate

The range in which the influence of the test movement rate on the K_{Ic} value could be examined was defined in advance by the capacity of the material testing machine. Critical stress intensity factors were measured in the case of eight traverse rates between 25 µm/min and 5000 µm/min. The values have been plotted in Figs. 25 and 26 against the logarithm of the movement rate. Fitted

curves were then calculated.

The slopes of the fitted curves differed only slightly from zero, i.e., K_{Iv} and K_{Imax} were virtually constant within the studied movement rate, although the statistical significance of this finding was not very good. The 95 % confidence limits for the estimated values show that it is perfectly possible for fitted curves with a positive or negative slope to occur (possible extreme positions for the 95 % probability are shown in interrupted lines). Marked variations in the fracture toughness values can therefore be expected in the case of movement rates a few orders of magnitude above or below those studied here.

A higher statistical significance does not appear a very urgent requirement at the moment, since no study results are at present available on the time history of the stress build-up during normal reactor operation. Estimates give reason to suppose that the relatively high movement rates, such as those occurring in the testing machine, will only be reached in the case of shutdown*). The only purpose of the above measurements, therefore, was to determine the influence of the movement rate in the experimentally feasible test procedure.

A test movement rate of 100 µm/min was adopted for all subsequent measurements. This represents a compromise between the possibility of observing the crack and the duration of a test.

---

*) The stress variation rates in the case of shutdown of the reactor are of an order of magnitude of 10^{-2} N/mm^2 sec (Ref. 35).

7.2.2 Influence of the Crack Length

The dependence of the fracture toughness on the relative crack length a/b was determined on specimens from electrodes I, II and III. Since it soon transpired that otherwise identical specimens, originating from different electrodes, gave clearly different measuring results (cf. paragraph 7.2.5), the electrodes were evaluated separately.

(a) Electrode II :

The specimens had sawn cuts between a/b = 0.3 and a/b = 0.7. The measured values have been plotted in graph form against the a/b ratio in Figs. 27 and 28. Fitted curves and the corresponding 95 % confidence limits were determined on the arbitrary assumption that the dependence was linear.

(b) Electrode I :

These specimens, in contrast to those from electrode II, were cut so as to conform to fixed values a/b $\approx$ 0.3, $\approx$ 0.5, $\approx$ 0.7. The three mean values for K_{Iv} have been plotted in Fig. 29 and those for K_{Imax} in Fig. 30. Fitted curves with 95 % confidence limits were determined from the individual measurements. The mean values for the three notch depths were relatively well positioned on the fitted curves. This may be regarded as evidence that the dependence of the fracture toughness values on the relative crack length is in fact linear within the studied range.

(c) Electrode III :

Here again we worked with fixed notch lengths of a/b $\approx$0.3 and a/b $\approx$ 0.7. The mean values with 95 % confidence limits for K_{Iv} have also been entered in Fig. 29 and those for K_{Imax} in Fig. 30.

A clear fall in the critical stress intensity factors with the crack length was found in all three electrodes. This contradicts the results of Corum (Ref. 24) and Yahr and Valachovic (Ref. 28), who found that the length of the crack exercised no influence. A more careful examination of the plots given by these authors, however, gives reason to assume a fall in the fracture toughness values with a/b within the range $a/b > 0.3$. The effect was not clearly visible as a result of the small numbers of specimens.

In view of the discrepancy between the present results and those of other authors, we determined the statistical probabilities of a reduction in the K_{Iv} and K_{Imax} values with a/b. In the case of the results for electrodes I and II this was done in the form of a confidence test for the slope. The specimens from electrode III with $a/b \approx 0.3$ and $a/b \approx 0.7$ were compared by the method of the comparison of two mean values. In almost all cases the probability of a reduction in the measured values with a/b was greater than 99.9 %. Only in the case of the K_{Iv} values of electrode II was a value of 96 % obtained (which still represents a high degree of certainty).

The attempt will be made below to interpret the described influence in terms of a volume effect.

The energies irreversibly consumed in a volume element are progressively higher, the higher the stresses in the element. No detailed information is available on

the exact stress distribution in the specimen, but it is known that the highest stresses occur in front of the tip of the crack, in the first place tensile and then compression stresses (cf. paragraph 7.2.3 and 7.2.4). With short crack lengths a relatively large specimen volume is exposed to high stresses, while with long cracks the highly stressed volume fraction is smaller. This results in a reduction in the dissipation of irreversible energies and the occurrence of a fall in the measured fracture toughness values with the crack length.

A rough diagrammatic representation of these facts is shown in Fig. 31. The hatched areas represent in this case the regions in which irreversible energies are most likely to be consumed.

A strength characteristic is required in the given situation for the most unfavorable conditions. This corresponds in the present case to a large crack length, i.e., a large a/b value. For this reason and in order to obtain independence of an arbitrary a/b value, one could use for comparison purposes a fracture toughness value extrapolated to a/b = 1. The extrapolation in graph form in Figs. 27-30 is yielded by the values in Table 5. It was found that the corresponding values K_{Iv} and K_{Imax} for the individual electrodes were virtually coincident in the case of a/b = 1. This was to be expected also, since with a theoretical crack length a:b = 1, covering the complete specimen, an incipient advance of the crack signifies also the breaking-through of the specimen.

7.2.3 Influence of Specimen Size

The influence of specimen size was studied on the basis of the geometrically similar specimen types Z 10, Z 30 and Z 60. Specimens Z 30 and Z 60 originated in this case from different electrodes and for Z 10 a mean value obtained from three electrodes was used therefore for the comparison (the mean values of the three electrodes were in this case very close together).

Table 6 shows the mean values of K_{Iv} and K_{Imax} with the corresponding standard deviations for the three specimen sizes. The rise in the fracture toughness values with specimen size is significant, the difference between Z 10 and Z 30 being greater in this case than between Z 30 and Z 60. Even in the latter case, however, statistical mean value comparisons indicate a certainty greater than 99.9 % for the rise in K_{Iv} and K_{Imax}.

The difference in the intensity of the rise (Z 10 → Z 30 and Z 30 → Z 60) can be better understood by comparing the effective volumes*). The volume ratio between specimen types Z 10 and Z 30 is 1:27 and between Z 30 and Z 60 it is still only 1 : 8.

---

*) The "effective specimen volume" is understood to mean that fraction of the total volume in which stresses can occur at all, i.e., the part between the line of the application of force and the rear edge of the specimen. The parts of the arms located in front of the line of the application of force are not subject to any stresses. The effective volume is given by V = bdl.

The values of K_{Iv} and K_{Imax} with the corresponding standard deviations have been plotted against the effective specimen volume in a logarithmic plot in Fig. 32.

The influence of specimen size can again be described by means of the consumption of irreversible energies. This consumption increases with the specimen volume, resulting in an increase in the fracture toughness.

For a more detailed examination of the influence of the volume on the fracture toughness, we have to differentiate between an increase in the volume in the form of the thickness of the specimen and in the form of an increase in the effective lateral surface area b.L.

If the stress conditions are considered over the thickness of the specimen, it may be assumed in the case of the specimen thicknesses used here in view of the low Poisson constants of the material (Seldin found values for the majority of graphites of ν = 0.10 to 0.15, (Ref. 36) that the two-dimensional strain state obtains over virtually the complete specimen. No change occurs therefore in the stress and strain conditions over the thickness of the specimen (apart from layers in the immediate vicinity of the surface). The irreversibly consumed energy, like the elastic energy released, increases in linear fashion with the thickness. Since, however, equation (27) relates to a thickness of "1", the measured fracture toughness values (provided that the condition of the two-dimensional strain state is fulfilled) must be independent of the specimen thickness.

With an increase in the specimen volume,

represented by an increase in the lateral surface area b.l (with a constant thickness), on the other hand, an increase in the fracture toughness can be expected. In view of the low threshold stress for irreversible processes in graphite (cf. Section 5), it is possible for irreversible processes to occur even in regions contained in a larger specimen - the consumption of irreversible energies being greater overall. The consequence of this is a rise in the fracture toughness with b.L. It has to be borne in mind, however, that the small specimen cannot be regarded as a section out of the large specimen.

The attempt will be made below to describe in diagrammatic form for two different sizes of specimen the pattern of stresses as a function of the distance from the tip of the crack. This pattern is dependent on the direction; two of the wide variety of possible directions have been selected for examination :

(a) Direction perpendicular to the fracture surface :

Only in the immediate neighborhood of the tip of the crack will the same increase in the stress occur in both specimens in the case of crack propagation. If the simplifying assumption is made that the stress falls in the direction of the surface to a value $\sigma = 0$, its curve can be plotted diagrammatically, as has been done in Fig. 33a. The areas below the curves (hatched regions) are a measure of the irreversible energy consumption.

(b) Direction in continuation of the fracture surface:

Here again the rise in the neighborhood

of the tip of the crack is identical in both specimens. An area of compression stresses*) occurs in the neighborhood of the rear edge of the specimen (Fig. 33b). The hatched areas in the drawing again represent the irreversibly consumed energies.

The rise in the fracture toughness values with the specimen volume, shown in Fig. 32, is clearly due therefore to the influence of the lateral area b.L. To confirm the hypothesis that the two-dimensional strain state applies in fact over the complete specimen and to determine the limiting thickness for this state, it is essential to carry out further fracture toughness tests on otherwise identical specimens of different thickness.

The influence of the specimen dimensions is of great practical importance. Since some of the structures in the reactor core are of an order of magnitude in which the effect makes itself felt very noticeably, it is not possible, for example, to base calculations for fuel element design on a fixed K_{Ic} value. The fracture mechanics concept can nevertheless be used in practice, if the exact dependence of the critical stress intensity factors on the specimen dimensions is known.

7.2.4 Influence of Prestressing

If a CT specimen is stressed with a constant increase in the strain beyond the maximum load, the crack length will increase in

---

*) This compression range was detected by Cords (Ref. 37) on a modified CT specimen, using a finite element technique. A hole was bored in the specimens at the end of the notch.

this case by an amount Δa. After relief and determination of the new crack length $a + \Delta a$, a fresh critical stress intensity factor can be recorded on the same specimen during application of a new load.

Tests of this type were carried out on several specimens, in each case until the crack increased to a relative length of $a/b > 0.7$ (limit of the validity range of the determination formula for K_I). Two examples of such measurements are shown in Fig. 34, in which the measured K_{Imax} values have been plotted against the relative crack length*). The initial crack length (notch length) of the two specimens differed in this case.

A clear rise in the measured fracture toughness values was recorded in all measurements. The rise was initially steep, but after a few applications of stress the curves merged into plateaus which were approximately 30 % above the initial value. In the case of very low stress rates a fall in the curve was even recorded after about 6-8 applications of stress (Fig. 35). The observed rise in the fracture toughness values agrees also with the observation of Yahr and Valachovic (Ref. 28) that a specimen, in which an incipient crack had been produced by the careful introduction of a chisel (i.e., a specimen stressed to immediately beyond the point of crack propagation)

---

*) The K_{Iv} values were not plotted, since their values were appreciably below the K_{Imax} values only in the case of the two first loads; from the third load onwards $K_{Iv} \approx K_{Imax}$.

had higher K_{Iv} values than a specimen with a sawn notch (i.e., without prestressing).

As was demonstrated in paragraph 7.2.2 on virgin specimens, the fracture toughness values decrease with the crack length a/b. This fact and the parallel course of the two curves in Fig. 34 prove that the increase in the a/b ratio cannot be held responsible for the observed effect.

It would be conceivable for the crack to advance further on the specimen surface than in the interior, which would simulate excessively high K_{Imax} values in the determination equation (27). If it is assumed, for example, that in curve II of Fig. 34 the K_{Imax} value determined during the first stress is valid for the subsequent stresses also, the crack on the surface would have to have advanced during the final stress 3.7 mm further than in the interior of the specimen. To check this point, a specimen was prestressed several times, cast in araldite and ground down layer by layer. A maximum difference of 1 mm was found in this case between the crack lengths at the surfaces and in the interior of the specimen. The increase in the fracture toughness values during the described experimental procedure is therefore undoubtedly a true prestressing effect.

The fall in the curve, occurring in Fig. 35 on the far side of a/b = 0.6, can hardly be a true result of the movement rate, but rather a consequence of the relatively frequent stressing of this specimen. It

was possible in this case in view of the low traverse rate of 25 µm/min to stop the machine relatively rapidly after reaching the maximum load. More measurements could therefore be recorded on this specimen within the range $0.3 \leq a/b \leq 0.7$ than in the specimens in Fig. 34 which were stressed at a higher rate. The conclusion may be drawn from the curve in Fig. 35 that two opposing effects are acting here : a nonlinear rise in the fracture toughness due to prestressing phenomena and a linear fall due to the increased crack length (cf. paragraph 7.2.2). After 6-8 stressing operations the first term clearly reaches saturation and the second effect predominates.

A physical explanation of the prestressing effect has again been sought on the basis of the known stress-strain behavior of graphite. As a result of application of the loads both tensile and also compression stresses occur in the material (cf. paragraph 7.2.3) and residual tensile and compression strains continue to apply in the corresponding regions. If extension of a crack has occurred during application of the load, a part of the region, which has undergone compression stresses during the previous application of the load, will now be exposed to tensile stresses as a result of the renewed application of the load (see Fig. 36). Additional energy has to be expended in order to "work out" the residual compression strains; this is reflected in an increase in the measured fracture toughness values.

7.2.5 Influence of the Electrode and Place from which the Specimen is obtained

It has already been pointed out that identical specimens from different electrodes have different K_{Iv} and K_{Imax} values. This phenomenon is due to differences in the production parameters, such as the graphitization temperature, compression pressure, precompression temperature, impregnation, etc. For comparison purposes, specimens from electrodes I and II underwent a comparative examination which was based on two different types of specimen (a/b = 0.3 and a/b = 0.7). The mean values together with standard deviations are given in Table 7. The values for electrode III are in this case 10 to 15 % below those for electrode I. A statistical mean value comparison confirms with a 99.9 % probability that there is a difference in the fracture toughness values of the two electrodes.

In order to examine the variations in the K_{Ic} value over the cross-section of an electrode, the K_I and K_{Imax} values were plotted for identical specimens in the corresponding planes from which the specimens were taken (Figs. 37 and 38). These specimens were type Z 30, a/b = 0.3 and Z 60, a/b = 0.5. In both cases a clear reduction in the fracture toughness by about 20 % was clearly recognizable from the edge to the center of the specimen. Particular note should be taken in this case of the continuous character of this reduction.

The reason for this effect is the increase in porosity from the edge to the center of the electrode due to the compression

process. If the pores and natural cracks in the material are regarded as an extension of the notch length, lower critical loads will be recorded in specimens from regions of lower density than in identical specimens from regions of higher density. Introduction of the same notch length a in equation (27) causes a reduction in the measured fracture toughness values in the direction from the edge to the center of the electrode. These effects of the electrode and of the site from which the specimen is taken amount to up to 20 %. It will therefore be necessary, when determining statistically significant fracture toughness values for graphite, to obtain the required specimens from different electrodes and from different positions within the electrode.

7.2.6 Influence of the Grain Size

Conventional tensile tests on similar types of graphite, differing only in their grain fractions, have shown that an increase in the grain size is accompanied by a decrease in the tensile strength (see Table 3). This gave reason to suppose that the fracture toughness would also be influenced by the grain size.

To clarify this question, ten specimens each were tested from material AS2-M-500 (maximum grain size : 3 mm) and material AS2-G-500 (maximum grain size : 10 mm). The mean values have been compared in Table 8 with those of comparable specimens from material AS2-F-500.

The fracture toughness values are clearly lower for the coarse-grained materials. The probability of a reduction in the fracture strength on changing from F to M material

was found by means of a statistical mean value comparison to be 99.9 %; the probability on changing from M to G material was > 90 %.

To explain this result, we have to regard the pores and natural cracks as an extension of the notch (cf. paragraph 7.2.5). The larger pores and cracks occur in the more coarse-grained materials. Introduction of identical notch lengths in equation (27) then results in a decrease in the fracture toughness values with an increase in the grain size.

7.3 The Critical Load

Determination of the fracture toughness requires in accordance with equation (27) a knowledge of the crack length and of the load at the moment of fracture. It is known from studies on other materials that the maximum load in the load-expansion curve is very much dependent on the test conditions and often yields overoptimistic values for K_{Ic} (cf. paragraph 3.3 and 3.4).

In graphite, crack propagation starts even before reaching the maximum load. The question now arises of whether this crack growth is to be regarded as critical, i.e., whether it can lead to fracture under unfavorable external conditions. The following test was carried out in connection with this problem.

Normal CT specimens were placed under a constant load which was between that required for incipient propagation of the crack P_v and the maximum load P_{max}. The crack opening, measured with an extension sensor, was recorded as a function of time. An additional expansion of the crack could be detected in this case

even a few hours after the start of the test. Under constant loads, the values of which were relatively close to the anticipated maximum load, a failure was recorded in several specimens after a maximum of 25 minutes. The time curve of the expansion of the crack in the specimen in this test has been plotted in Fig. 39.

This experiment shows that the maximum load of the load-expansion curve yields over-optimistic fracture toughness values with the relatively high test movement rates used here. The resulting requirement for a very much slower application of the load cannot be met on grounds both of equipment capacity and time.

It is not yet possible to give a final answer to the question of whether in the fracture toughness test the use of crack expansion can replace determination of the critical load as a criterion of the fracture toughness. For this purpose it will be necessary to examine whether every specimen fails under a constant load $P > P_v$ after a sufficiently long waiting time. This will require systematic stress/time to fracture tests with more suitable equipment and under constant and undisturbed test conditions.

8. Summary and Conclusions

An attempt has been made in the present paper to apply data from linear-elastic fracture mechanics to graphite. It has been found that the basic requirement of a predominantly linear-elastic stressing of the specimen cannot be met in the case of graphite. This is due to the quasi-plastic residual strain values which have to be

interpreted predominantly as crack expansion. These "graphite-plastic" deformation phenomena occur in the complete specimen volume which is under stress and result in a pronounced dependence of the measured fracture toughness values on the geometrical parameters. No generally valid K_{Ic} value can therefore be given as a material characteristic for graphite. The fracture toughness concept can nevertheless be applied, if the critical K_I values are known as a function of geometrical parameters.

Apart from the influence of the geometrical factors, the fracture toughness values are very much influenced by production parameters. Different values are recorded depending on the site from which the specimen is taken, the electrode and the grain size.

The test rate v does not affect the K_{Iv} and K_{Imax} values within the range studied ($0.25\ \mu m/min \leq v \leq 5\ mm/min$). There are indications, however, that lower critical stress intensity factors can be expected in quasi-static tests.

The most urgent task in future fracture toughness investigations is to clarify the question of whether incipient crack expansion can be related to the critical load for quasi-static loading. This will require stress/time to fracture tests under a cover gas atmosphere in shock-free, temperature-stabilized rooms. A closer study of the crack propagation conditions appears desirable. An attempt should be made to determine the limiting thickness for the two-dimensional strain state by measurements on otherwise identical CT specimens of different thickness.

In the present paper only specimens obtained in accordance with scheme Z were tested (see

Fig. 14). Measurements on specimens from the other cross-sectional directions X and Y are still required.

The temperature behavior of the critical stress intensity factors is also of course important in connection with use in the core of a high-temperature reactor. It is desirable to carry out fracture toughness measurements under HTR operating conditions also, starting with unirradiated specimens. The influence of corrosive gases should also be checked in this connection.

After this work has been completed, a start will have to be made with fracture toughness studies on irradiated specimens.

Since graphite is also subject in the reactor to a number of cyclic stresses, we need to know, in addition to the aspects referred to above, how far cyclic stresses influence crack propagation in graphite. Before this can be done, the general cyclic stress behavior or graphite will have to be established in the form of stress/cycle diagrams.

The attempt made here to apply the fracture toughness concept to graphite has been found to provide an approach to a better understanding of the strength behavior and fracture conditions of graphite - even if the measured K_{Iv} and K_{Imax} values cannot at present be used in the practical safety analysis of graphite reactor components.

		"	⊥
Dichte	(kg/m^3)	2266	
E-Modul	(N/mm^2)	$\approx 10^6$	$\approx 3{,}5 \cdot 10^4$
Wärmeleitfähigkeit	(W/m K)	>400	≈8
Spez. el. Widerstand	(Ω mm^2/m)	≈0,5	$\approx 10^4$

Tab. 1: Physikalische Eigenschaften des Graphit-Einkristalls parallel (") und senkrecht (⊥) zu den Schichtebenen.

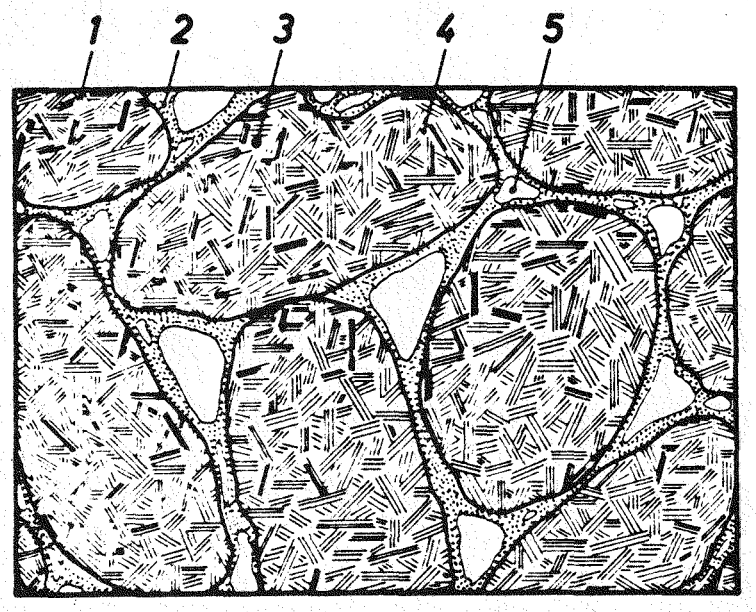

Abb. 2: Schematischer Schnitt durch einen polykristallinen Graphit (nach (2)).
1: Kristallit, 2: Binder, 3: Korn,
4: Mikropore, 5: Makropore.

		"	⊥
Rohdichte	(kg/cm^3)	1760	
Spez. el. Widerstand	(Ω mm^2/m)	8,3	10,3
Dyn. E-Modul	(N/mm^2)	10^4	$8{,}3 \cdot 10^3$
Zugfestigkeit	(N/mm^2)	12,8	11,3
Therm. Ausdehnungskoeff.	(K^{-1})	$3{,}6 \cdot 10^{-6}$	$4{,}5 \cdot 10^{-6}$
Wärmeleitfähigkeit	(W/m K)	169	140

Tab. 2: Physikalische Eigenschaften eines Reaktorgraphits (Typ: AS2-F-500)
": parallel, ⊥: senkrecht zur Preßrichtung.

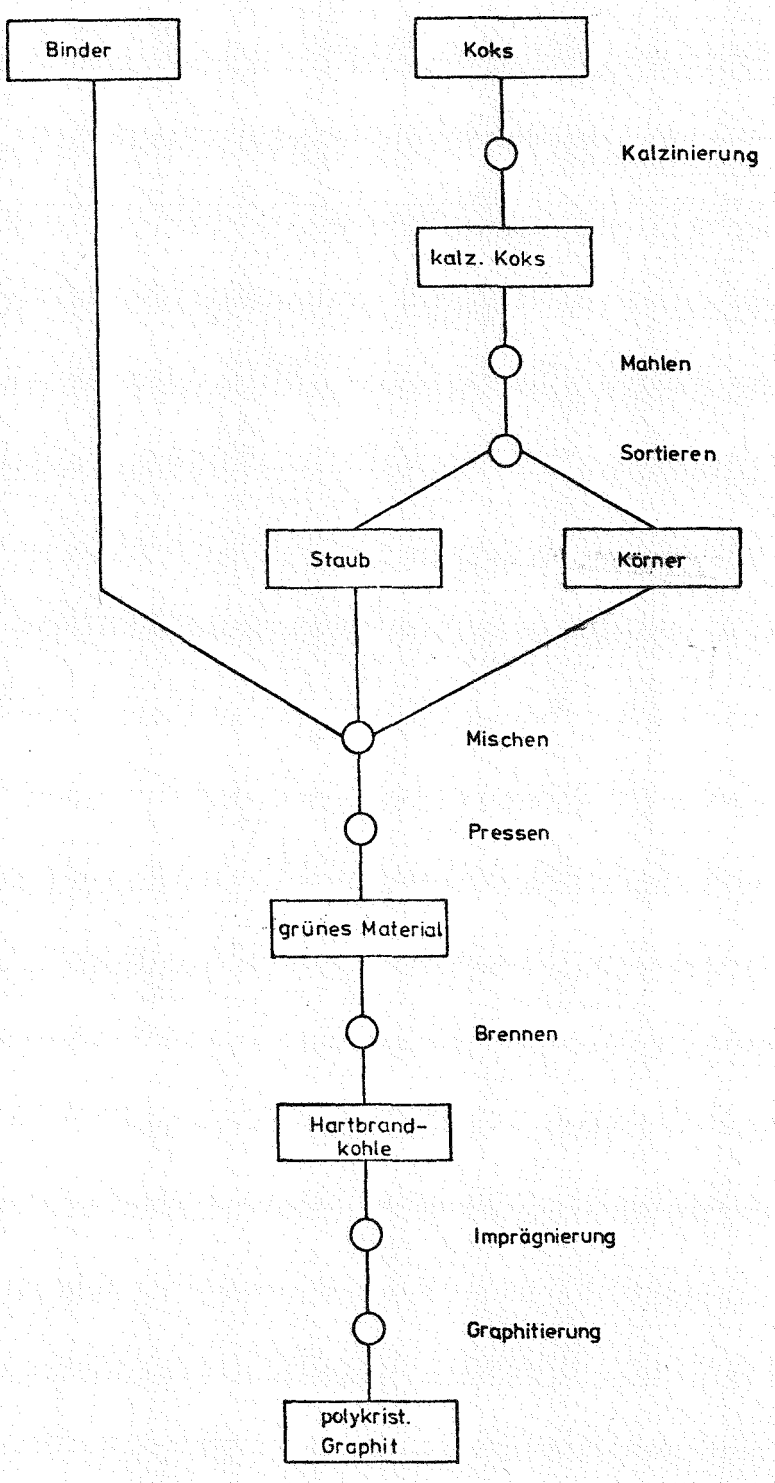

Abb. 3: Technische Herstellung eines polykristallinen Graphits (aus (3))

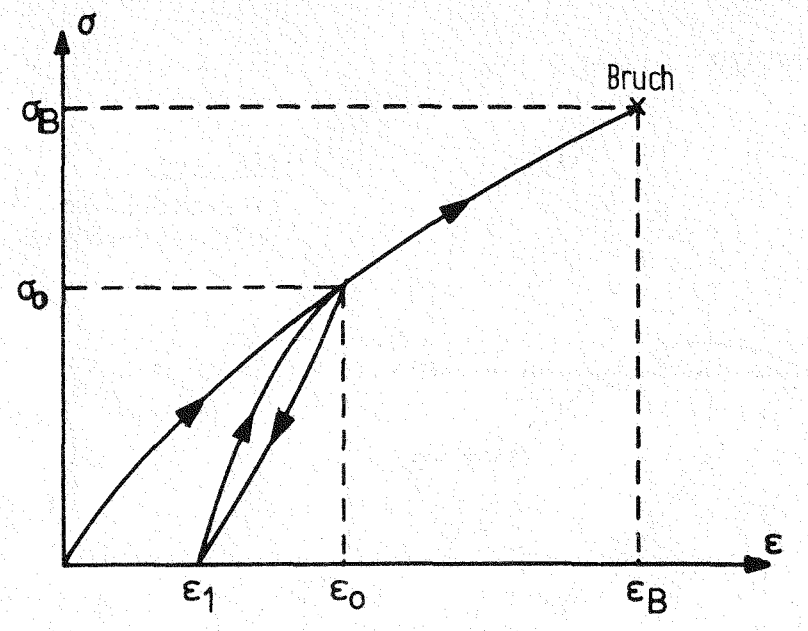

Abb. 4: Spannungs-Dehnungs-Charakteristik von Graphit

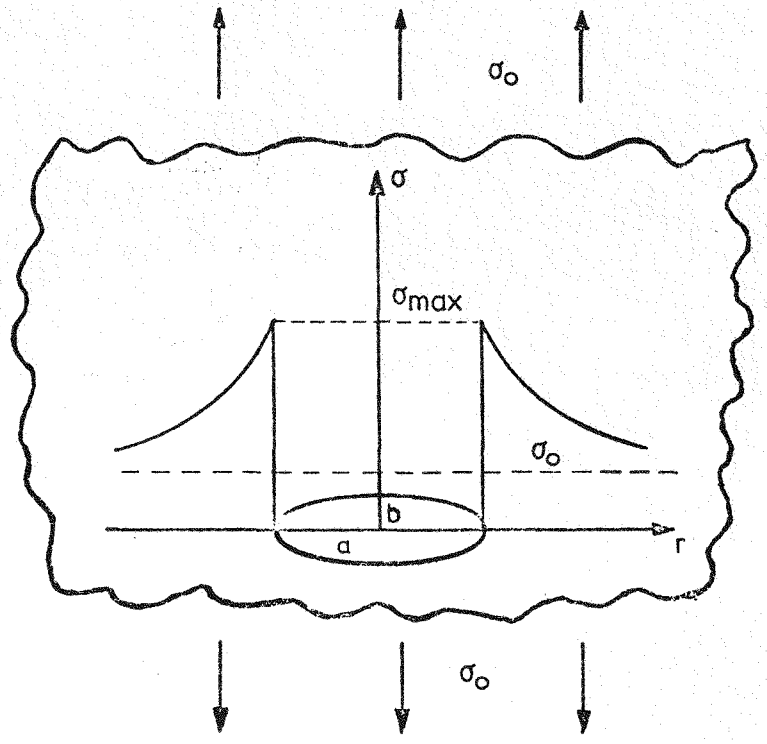

Abb. 5: Spannungsanstieg auf der x-Achse in der Nähe eines elliptischen Risses bei einer äußeren Spannung σ_o

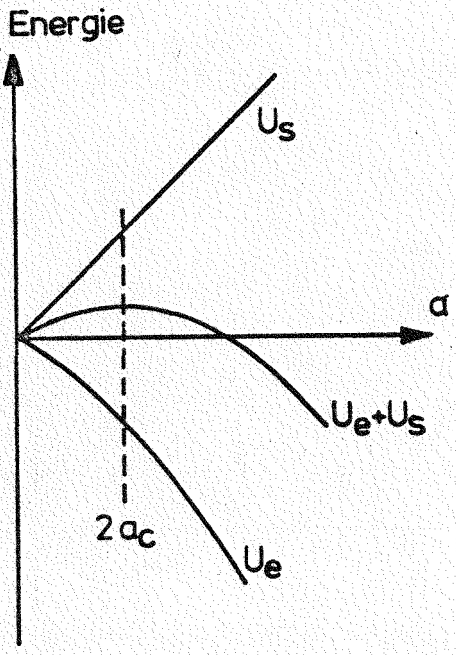

Abb. 6:
Energiebilanz für Rißausbreitung

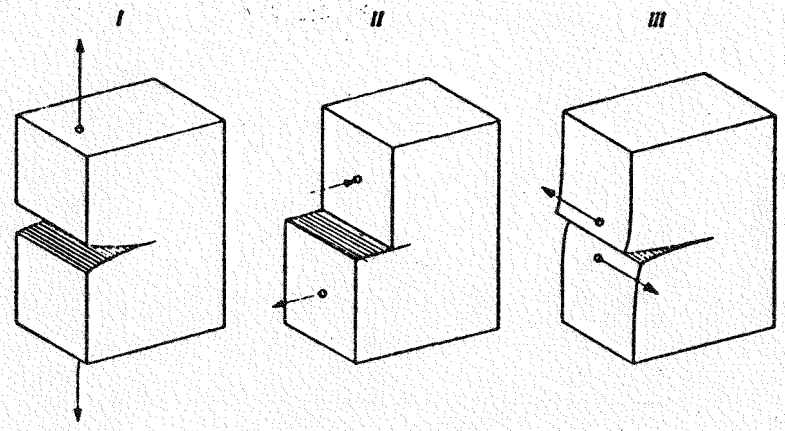

Abb. 7: Beanspruchungsarten an der Rißspitze (aus (15))

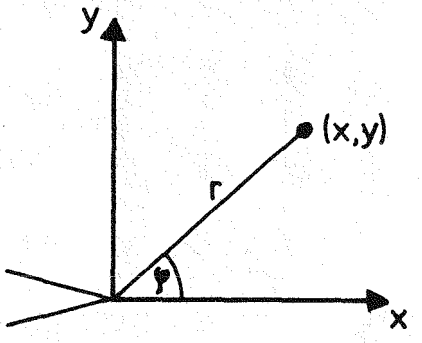

Abb. 8:

Beschreibung eines Punktes (x,y) vor der rechten Rißspitze in Polarkoordinaten

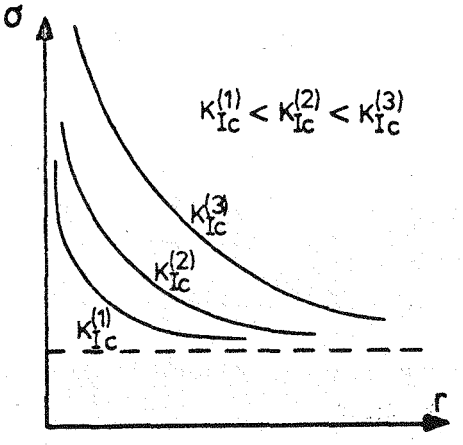

Abb. 9:

Spannungsüberhöhung vor der Rißspitze in einer unendlich großen Platte für drei verschiedene Spannungsintensitätsfaktoren

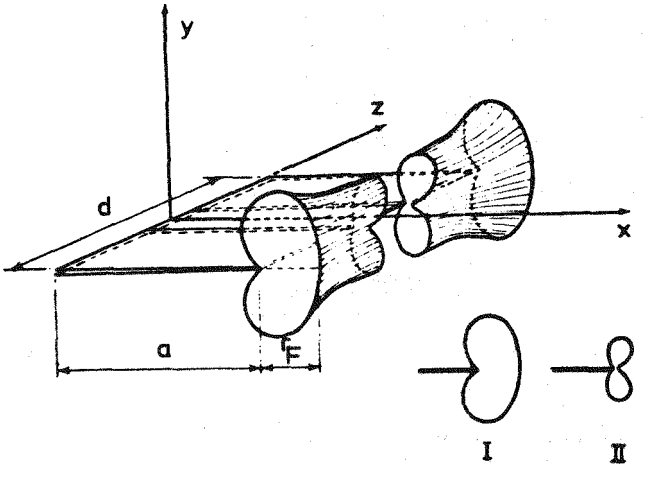

Abb. 1o: Plastische Zone an der Rißspitze; I: ebener Spannungszustand, II: ebener Dehnungszustand (aus (7))

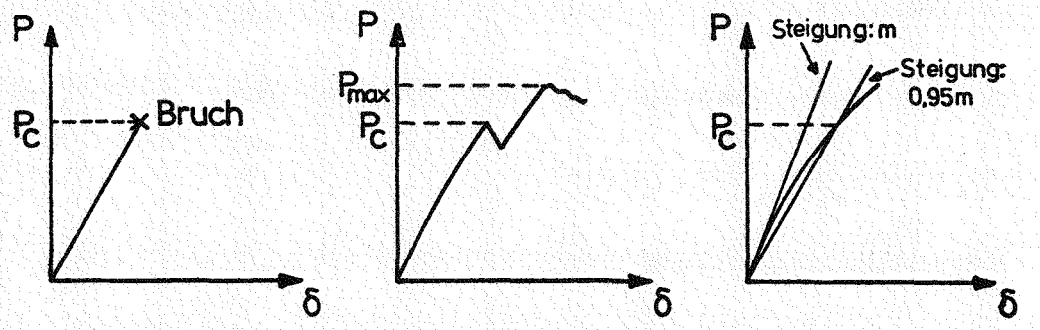

Abb. 11: Last-Aufweitungs-Diagramme: a) ideal-sprödes Verhalten, b) kritische Last aus dem "pop in", c) 5% Sekanten-Methode.

			AS2-F-5oo	AS2-M-5oo	AS2-G-5oo
Wahre Dichte	(Kg/m^3)		219o	22oo	22oo
Rohdichte	(Kg/m^3)		176o	172o	171o
Dyn. E-Modul	(N/mm^2)	"	$1o^4$	$1o^4$	$1o^4$
		⊥	$8 \cdot 1o^3$	$8 \cdot 1o^3$	$8 \cdot 1o^3$
Zugfestigkeit	(N/mm^2)	"	13	12	11
		⊥	11	9	9
Biegefestigkeit	(N/mm^2)	"	23	2o	18
		⊥	18	16	13
Druckfestigkeit	(N/mm^2)	"	51	45	4o
		⊥	5o	45	35

Tab. 3: Mechanische Kenngrößen der Graphite AS2-F-5oo und AS2-M-5oo

d	b	b_1	L	S	H	a	N
6o	12o	15o	144	66	25	vgl.	
3o	6o	75	72	33	15	Kap. 5.3.2	
1o	2o	25	24	11	5		

Tab. 4: Abmessungen der CT-Proben in mm (vgl. Abb. 12)

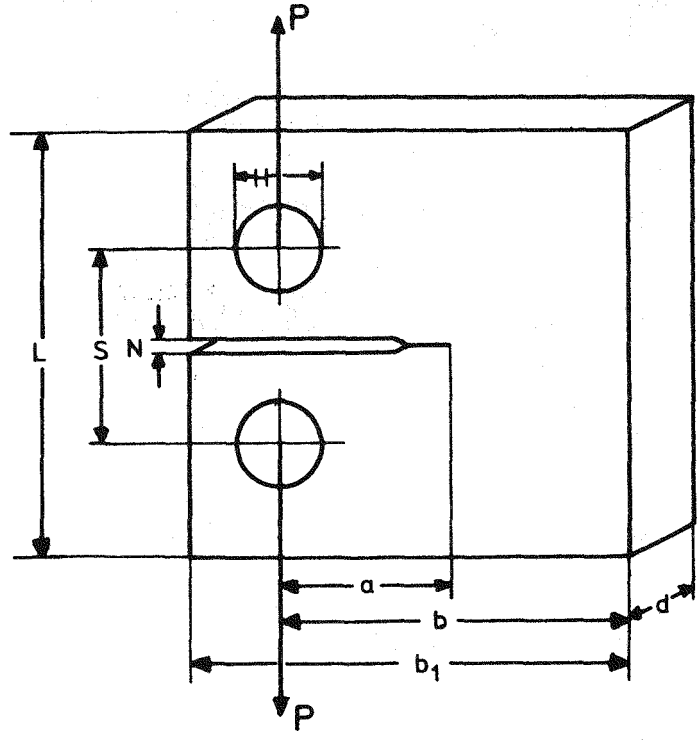

Abb. 12: CT-Bruchmechanikprobe

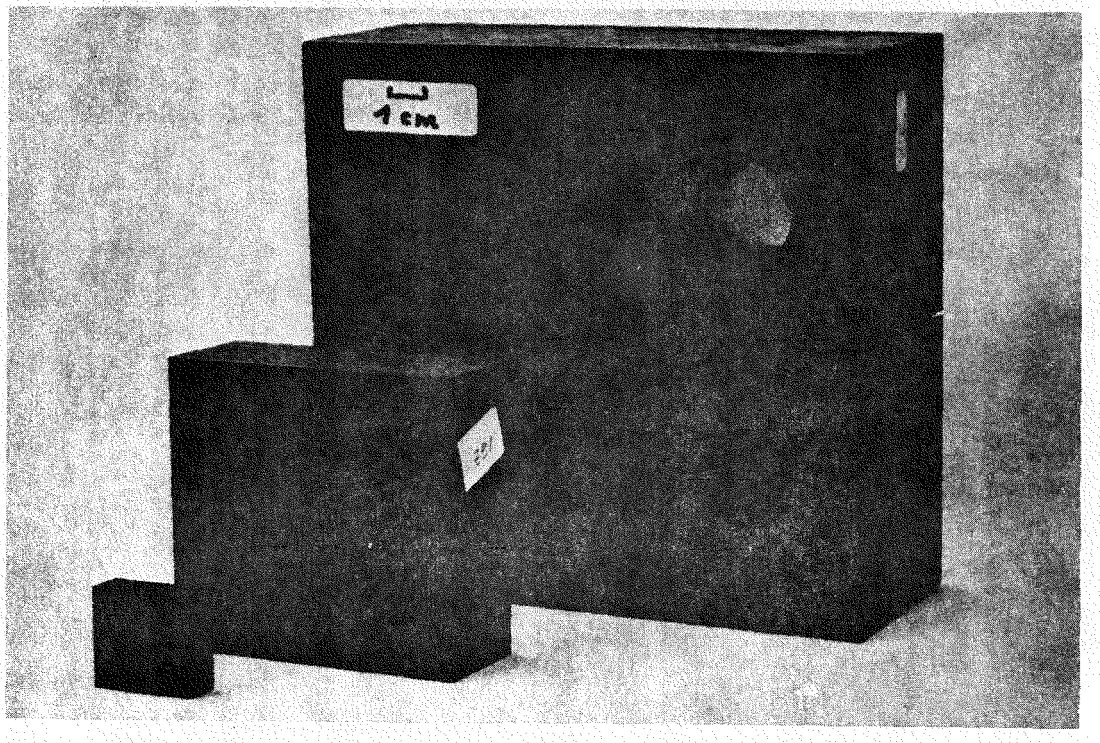

Abb. 13: CT-Proben aus Graphit

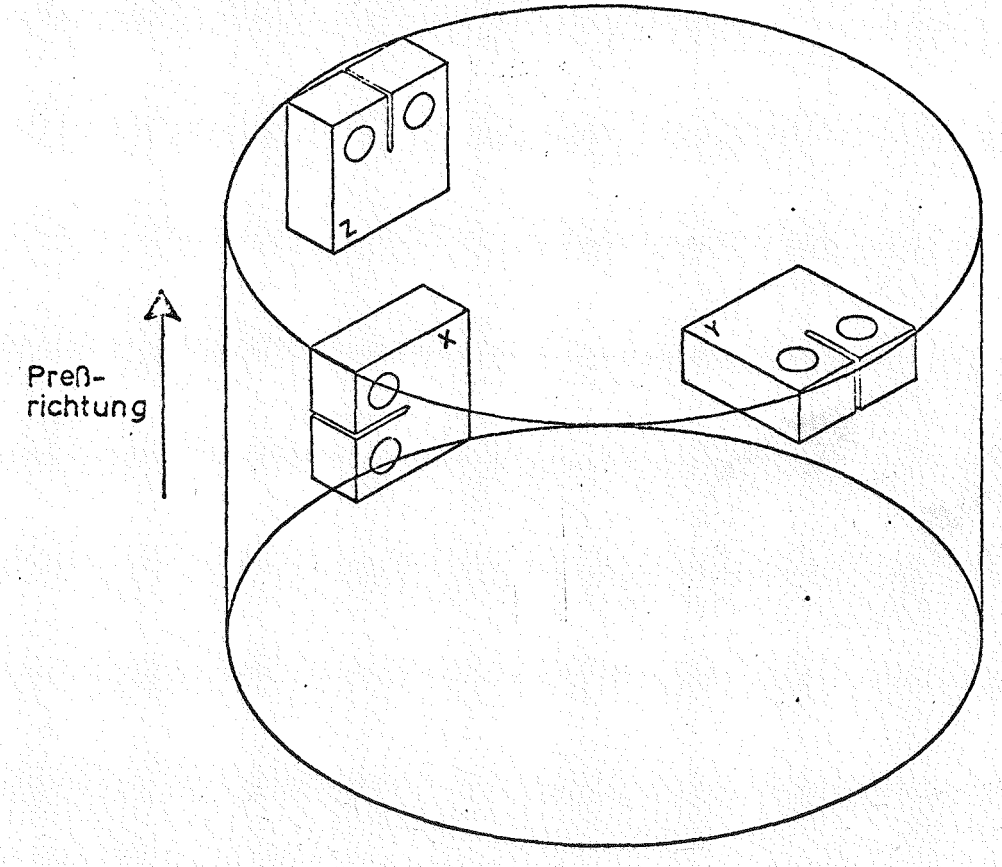

Abb. 14: Entnahme von CT-Proben aus stranggepreßten Graphitblöcken

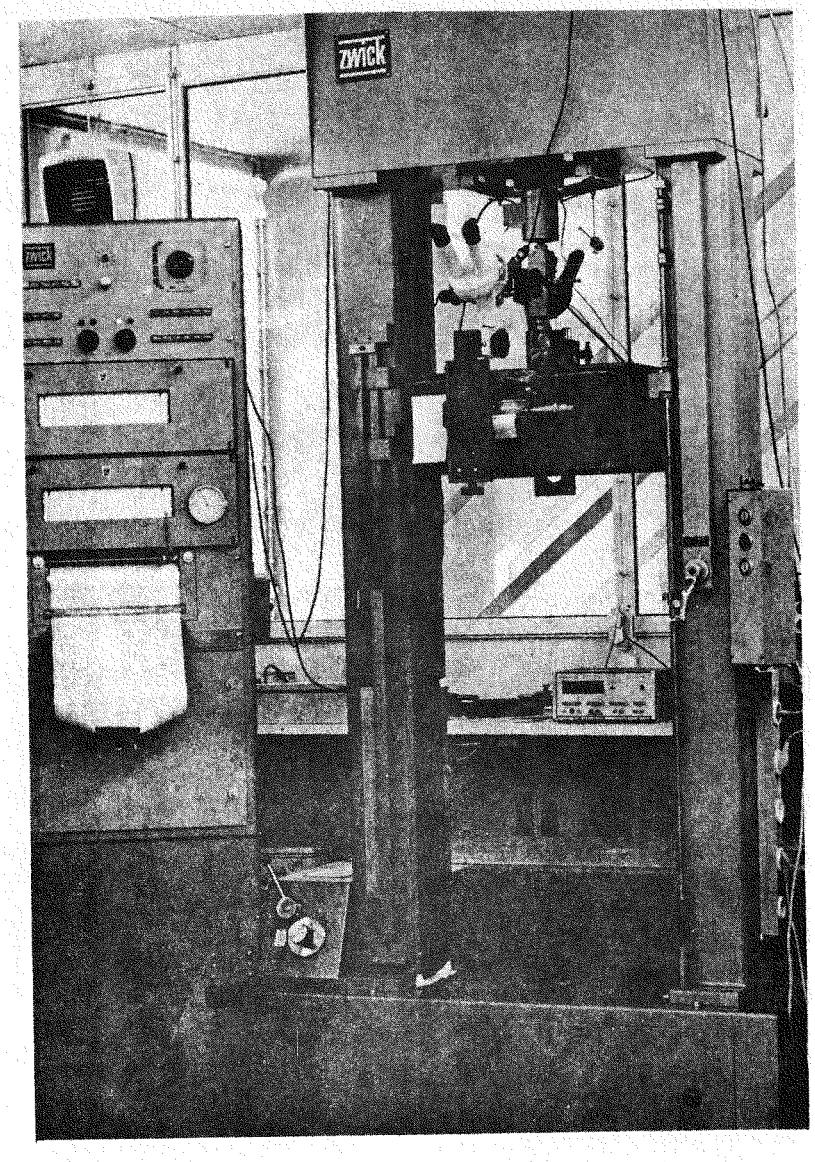

Abb. 15: Materialprüfmaschine Zwick 1385

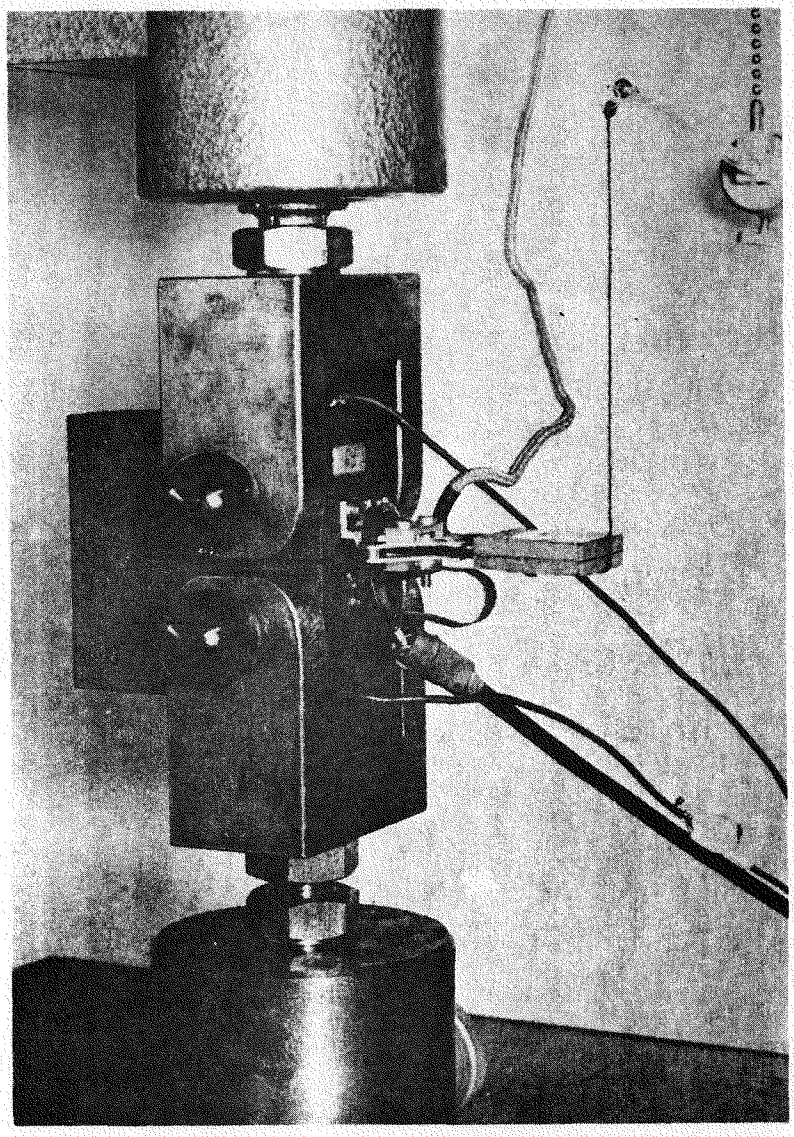

Abb. 16: Probenaufhängung in der Materialprüfmaschine

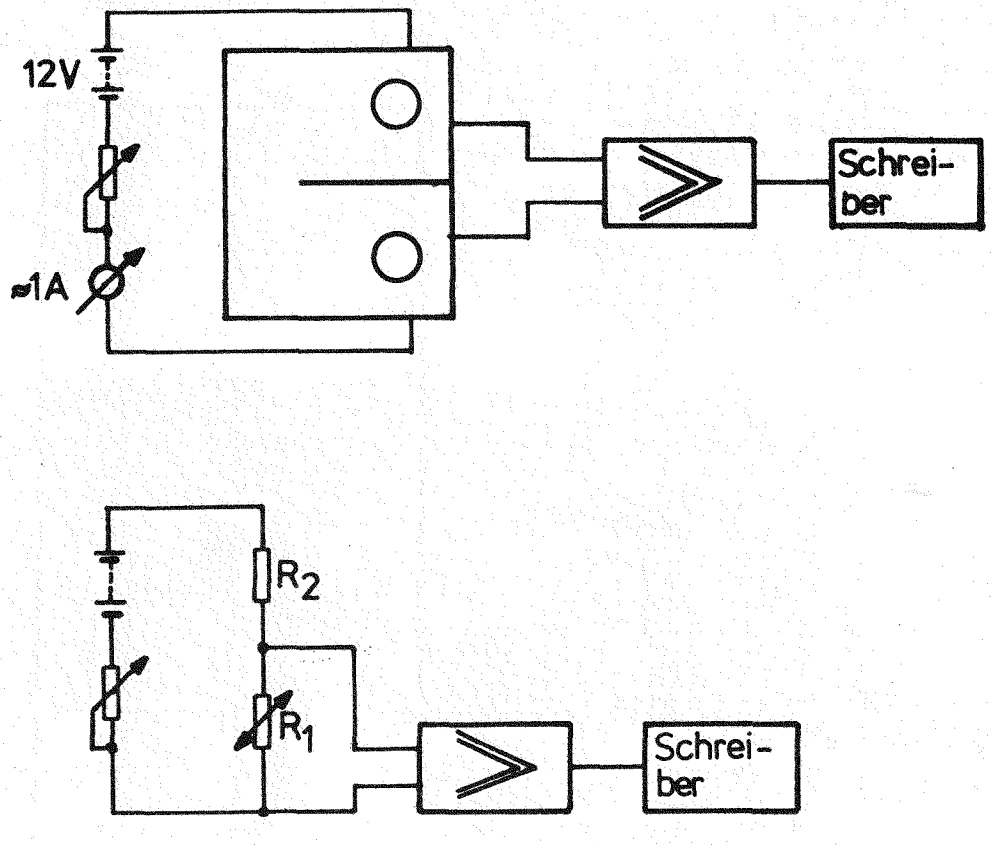

Abb. 17: Elektrische Potentialmethode zur Bestimmung des Rißeinsatzes.
a) Aufbau b) Ersatzschaltbild

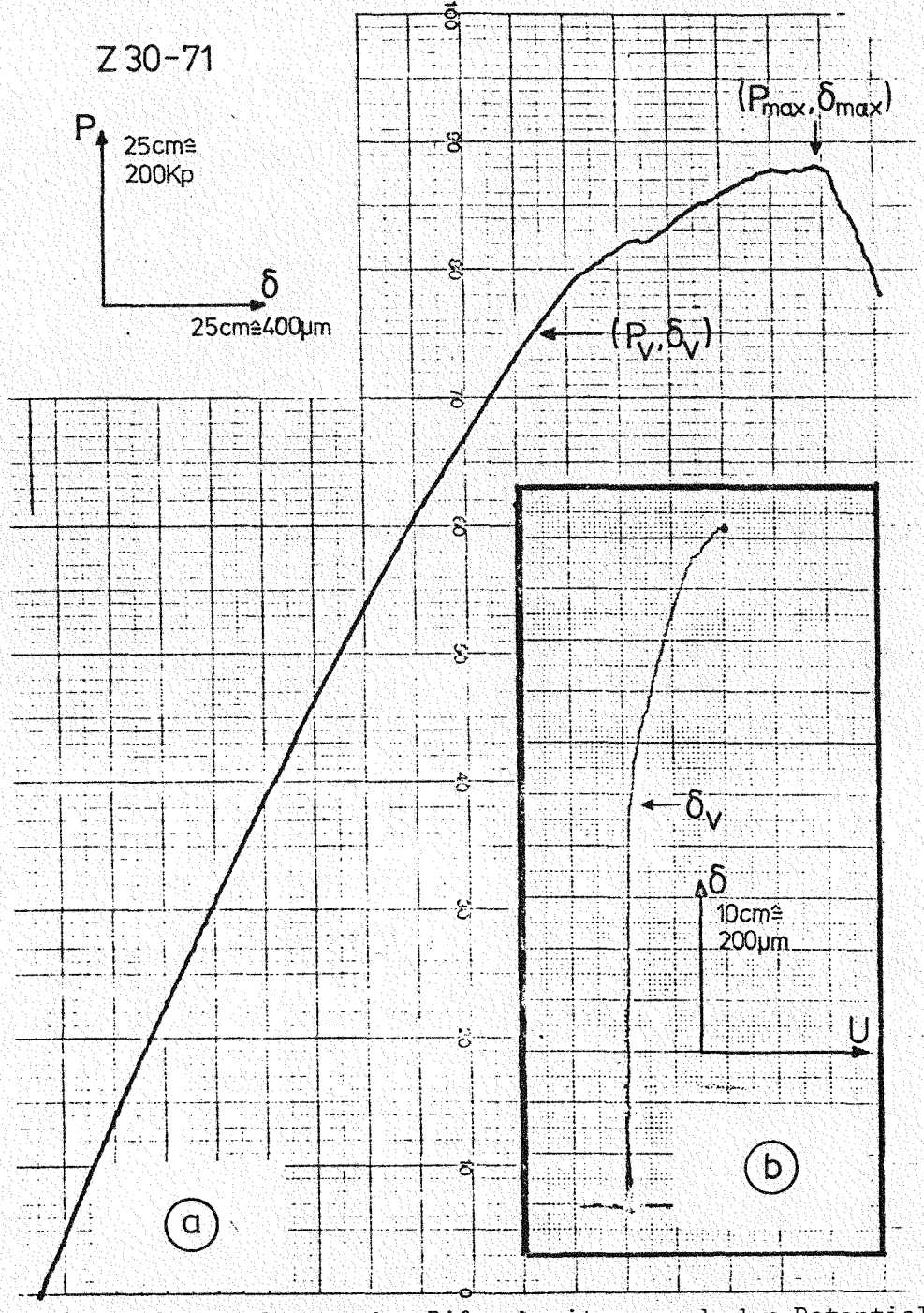

Abb. 18: Bestimmung der Rißausbreitung nach der Potentialmethode. a) Last-Aufweitungs-Kurve, b) Potential-Aufweitungs-Kurve

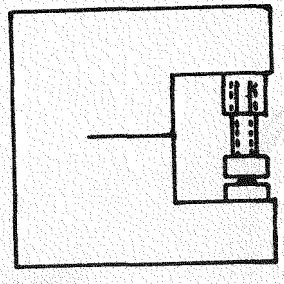

Abb. 19:

Anordnung zur Aufweitung von Graphitproben

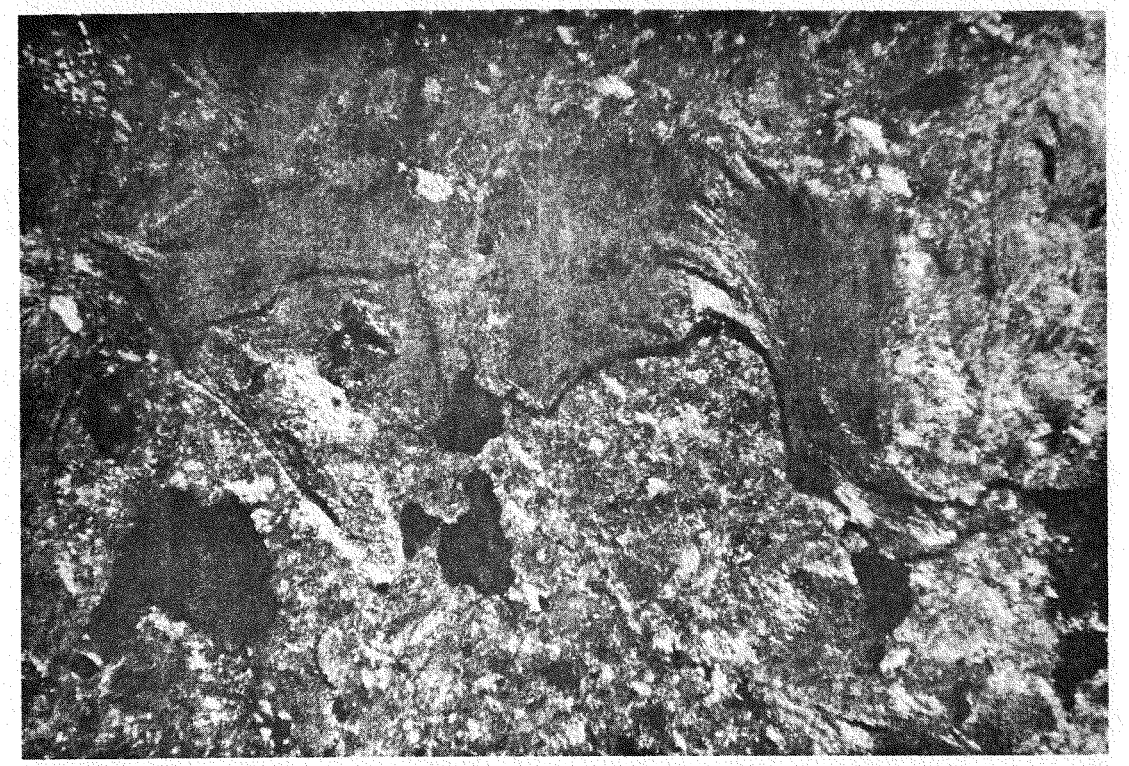

Abb. 2o: Aufnahme eines Risses in polarisiertem Licht (Vergrößerung: 5o x)

Abb. 21: Ablenkung des Risses durch ungünstig liegendes Korn (Vergrößerung: 1oo x)

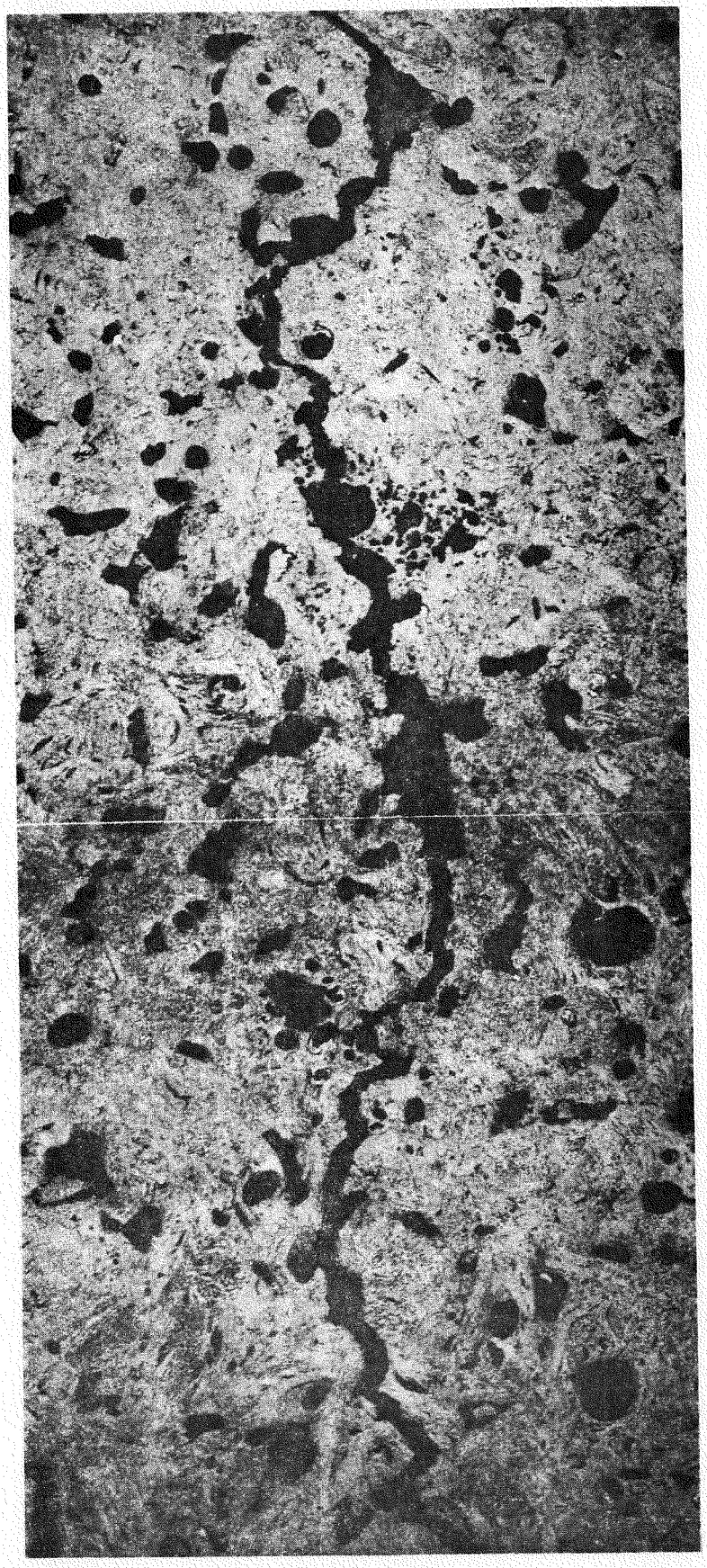

Abb. 22:

Bruchverlauf in
Graphit
(Vergrößerung: 2o x)

Abb. 23: Bereich in der Nähe der Rißspitze
(Vergrößerung: 5o x)

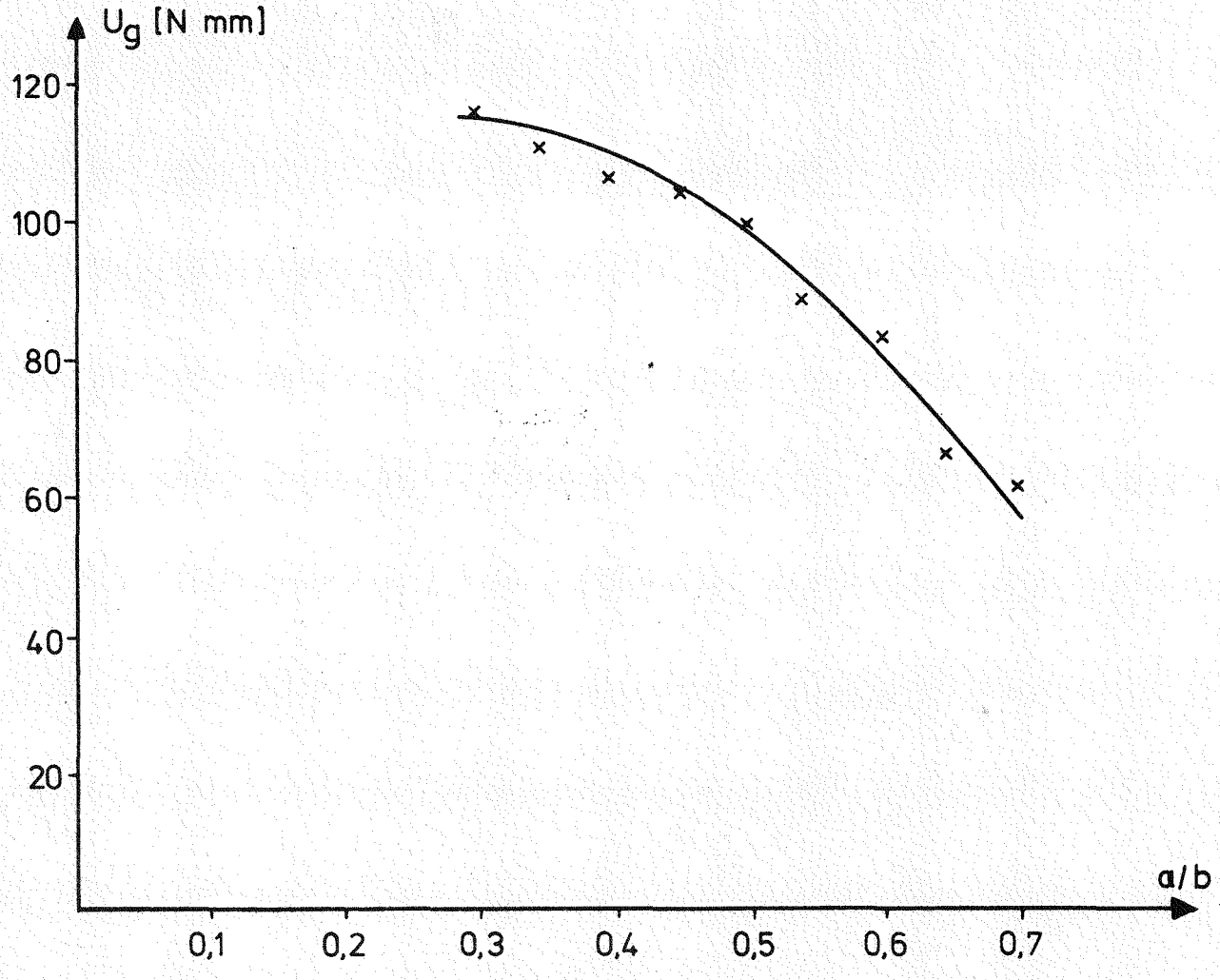

Abb. 24: Verlauf der in der Probe gespeicherten Energie mit der Rißlänge

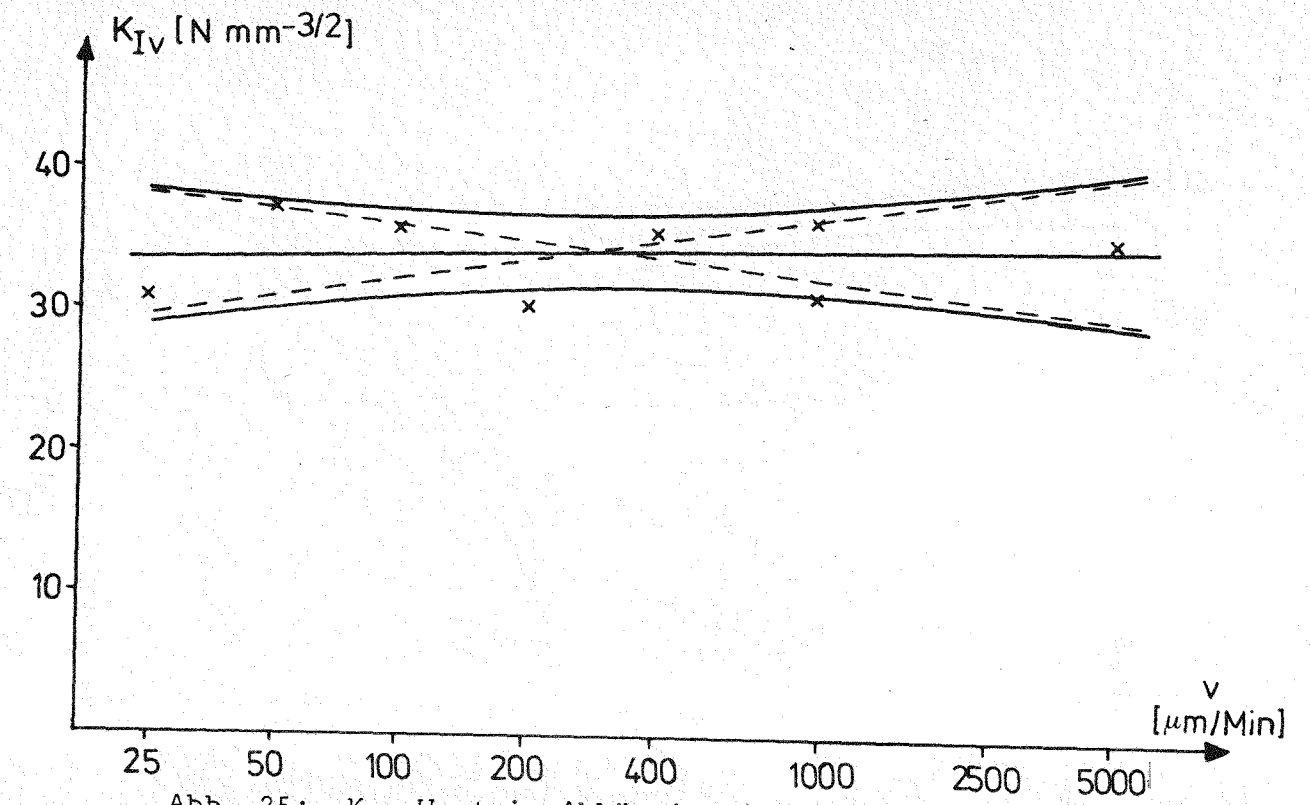

Abb. 25: K_{Iv}-Wert in Abhängigkeit von der Versuchsgeschwindigkeit (mit 95% Vertrauensgrenzen)

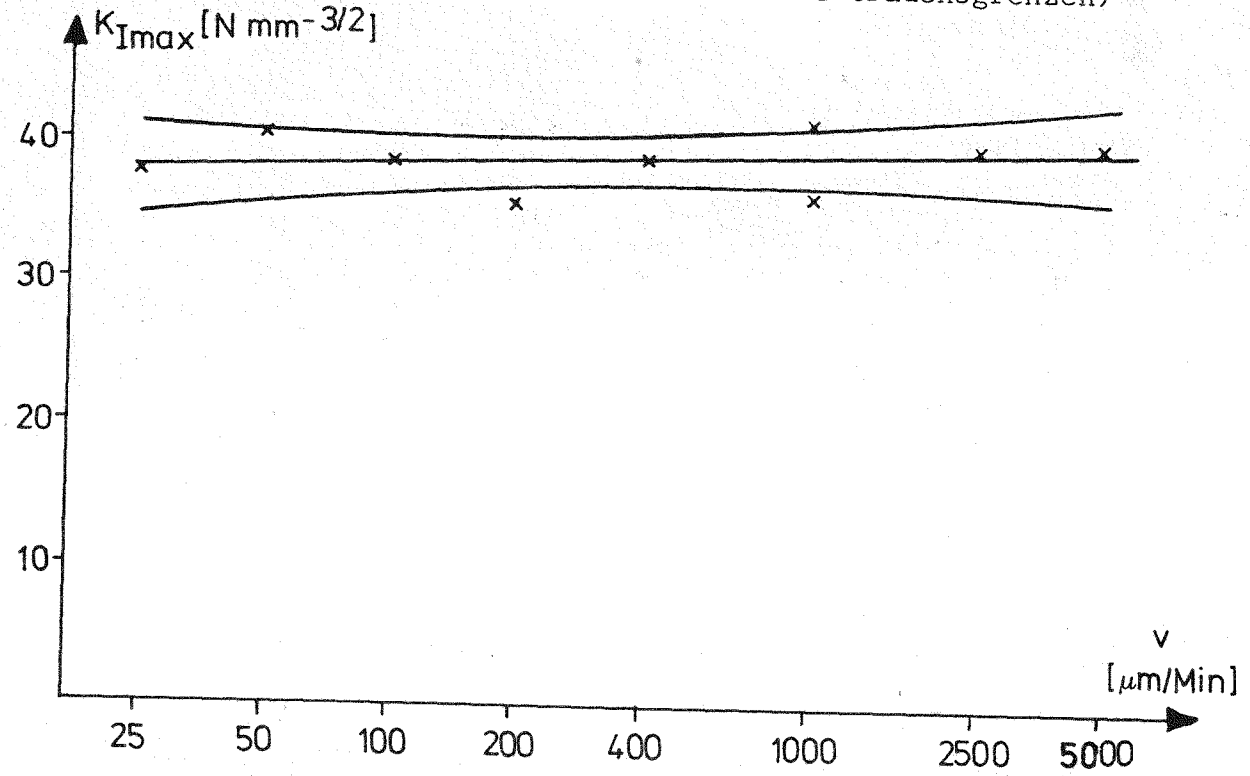

Abb. 26: K_{Imax}-Wert in Abhängigkeit von der Versuchsgeschwindigkeit (mit 95% Vertrauensgrenzen)

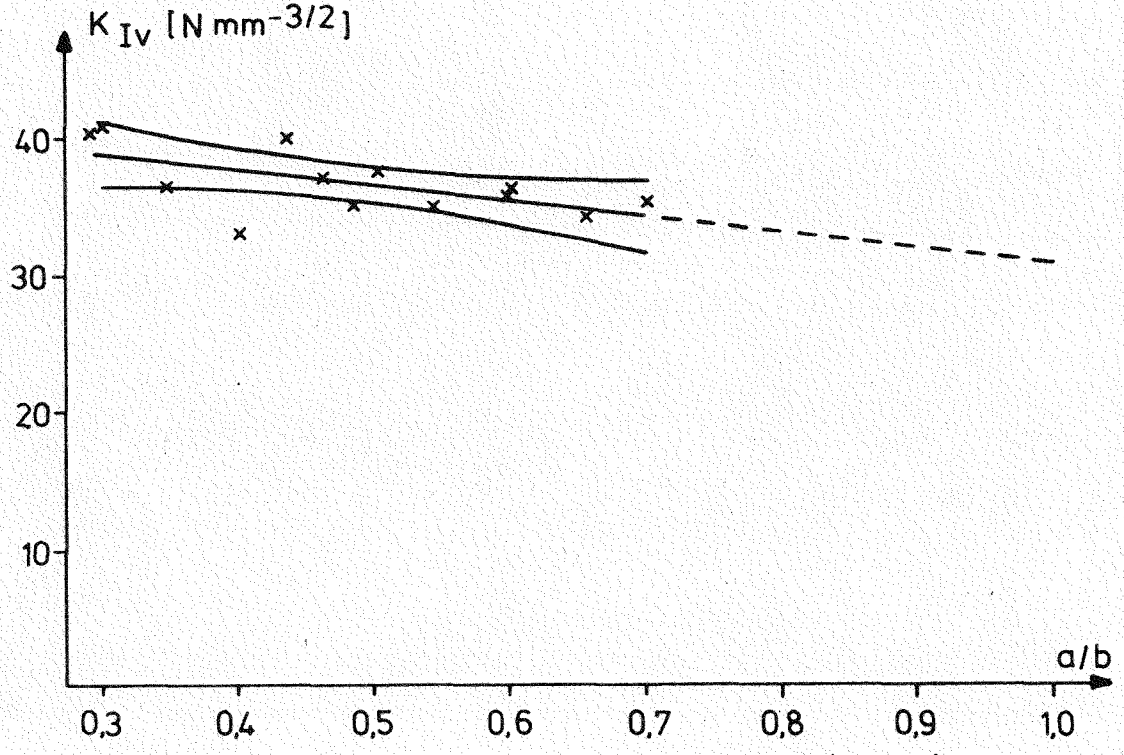

Abb. 27: K_{Iv}-Wert als Funktion der relativen Rißlänge a/b mit 95% Vertrauensgrenzen (Elektrode II)

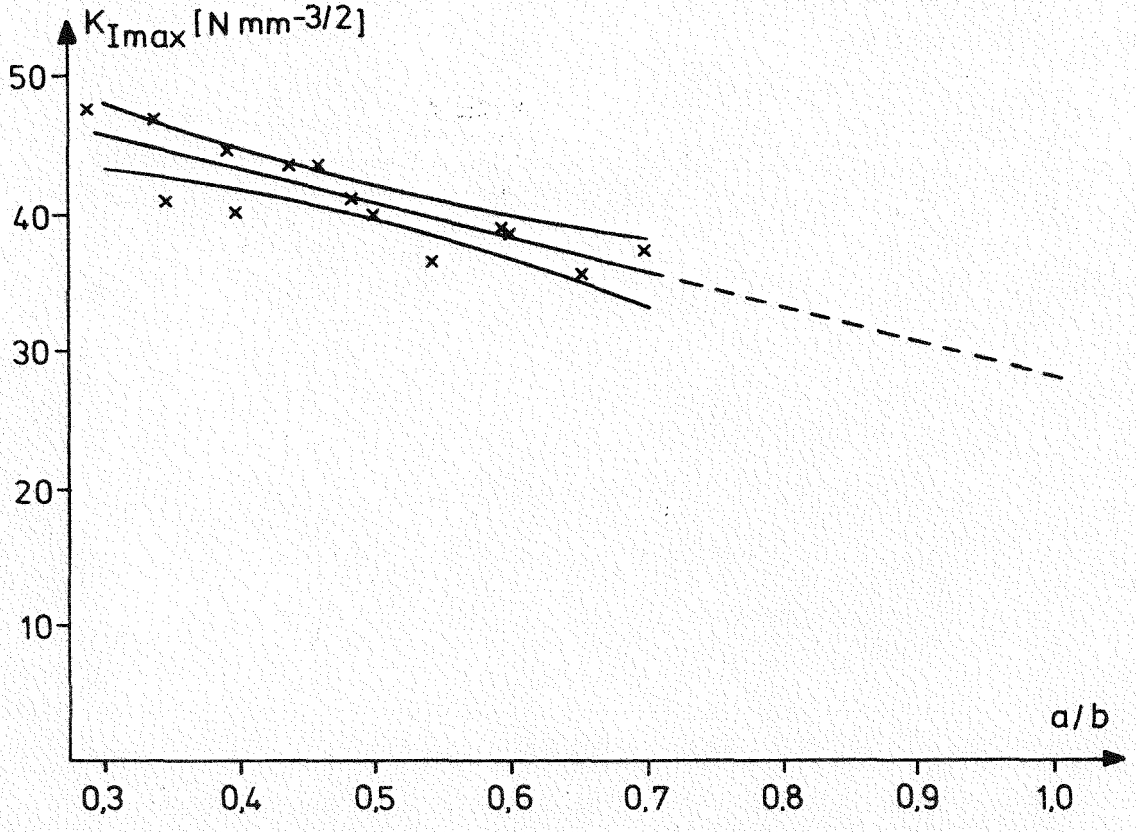

Abb. 28: K_{Imax}-Wert als Funktion der relativen Rißlänge mit 95% Vertrauensgrenzen (Elektrode II)

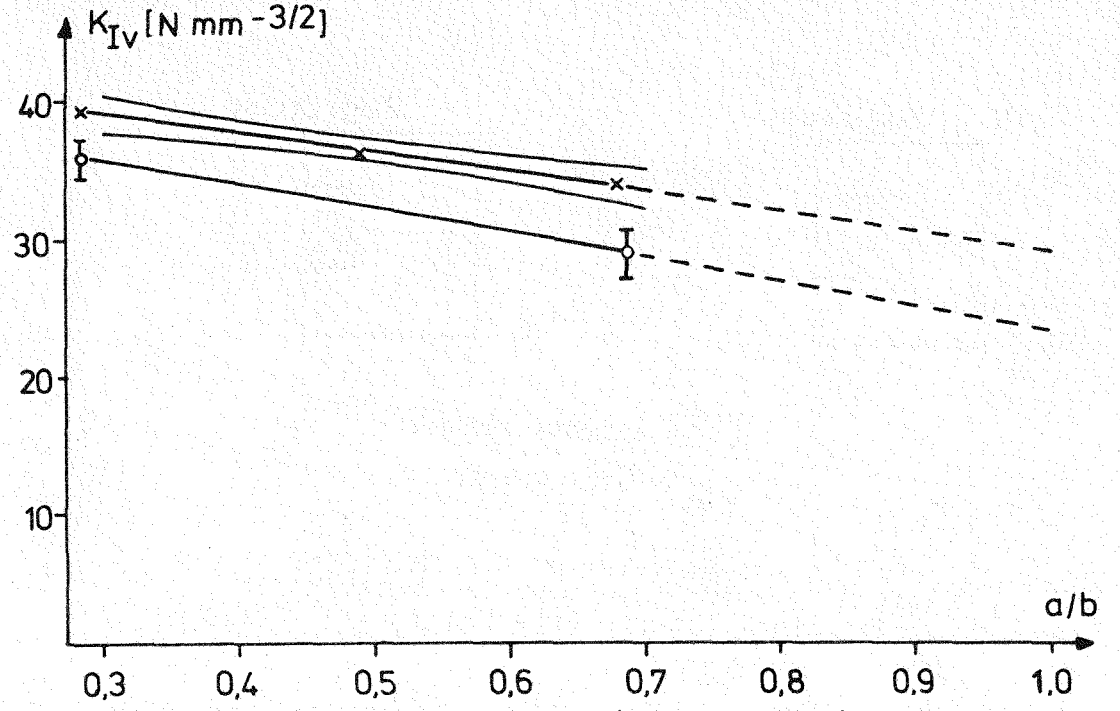

Abb. 29: K_{Iv}-Werte als Funktion der relativen Rißlänge a/b mit 95% Vertrauensgrenzen (x: Elektrode I, o: Elektrode III)

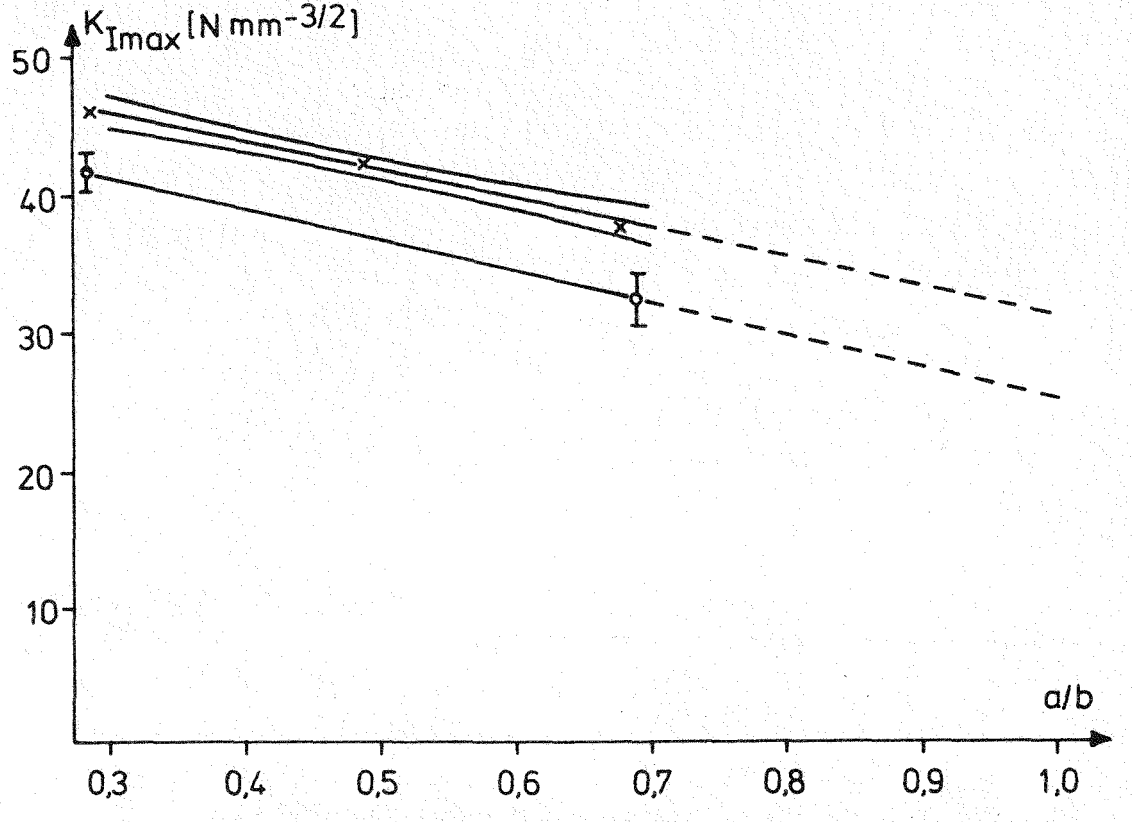

Abb. 3o: K_{Imax}-Werte als Funktion der relativen Rißlänge a/b mit 95% Vertrauensgrenzen (x: Elektrode I, o: Elektrode II)

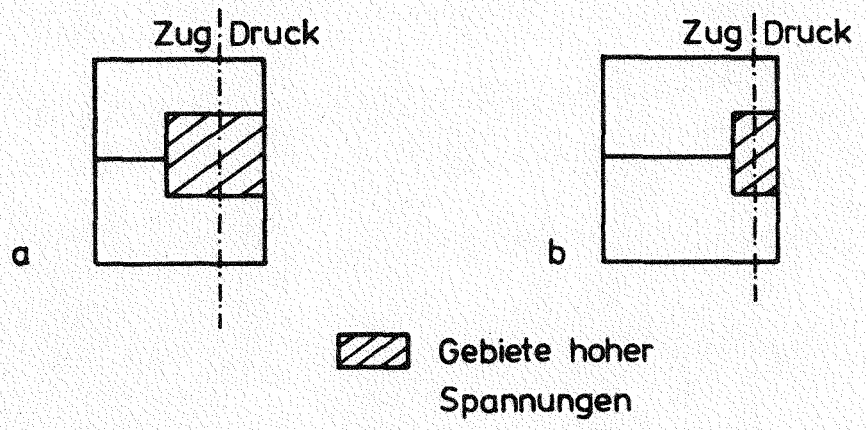

Abb. 31: Schematische Darstellung der Bereiche bevorzugten irreversiblen Energieverbrauchs in CT-Proben. a) kurzer Einschnitt, b) tiefer Einschnitt.

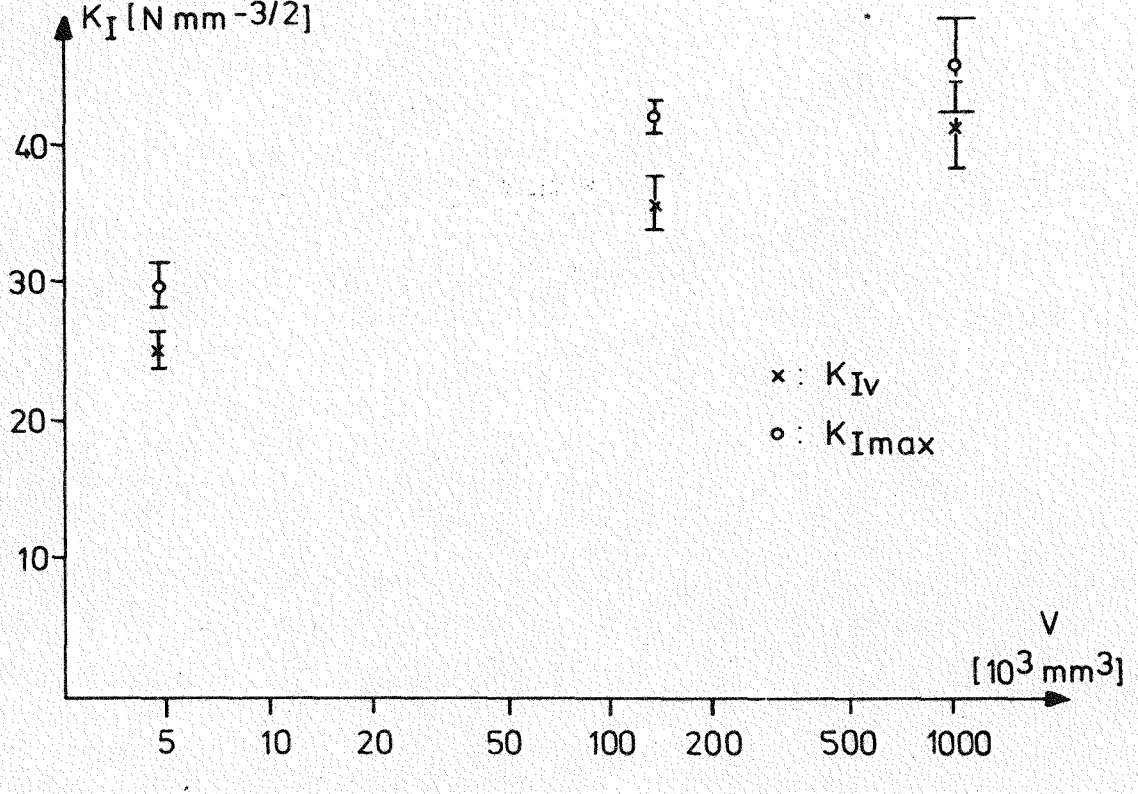

Abb. 32: K_{Iv} und K_{Imax} als Funktion des wirksamen Probenvolumens

	K_{Iv} $(N/mm^{-3/2})$	K_{Iv} $(N/mm^{-3/2})$
Elektrode I	28,6	3o,9
Elektrode II	3o,5	27,7
Elektrode III	27,7	25,o

Tab. 5: Auf a/b = 1 extrapolierte K_{Iv}- und K_{Imax}-Werte

		Z 1o	Z 3o	Z 6o
K_{Iv}	$(N/mm^{-3/2})$	24,6 ± 1,4	35,6 ± 2,o	41,3 ± 3,o
K_{Imax}	$(N/mm^{-3/2})$	3o,o ± 1,6	42,o ± 1,1	45,8 ± 3,4

Tab. 6: Gegenüberstellung von K_{Iv}- und K_{Imax}-Werten verschiedener Probengrößen

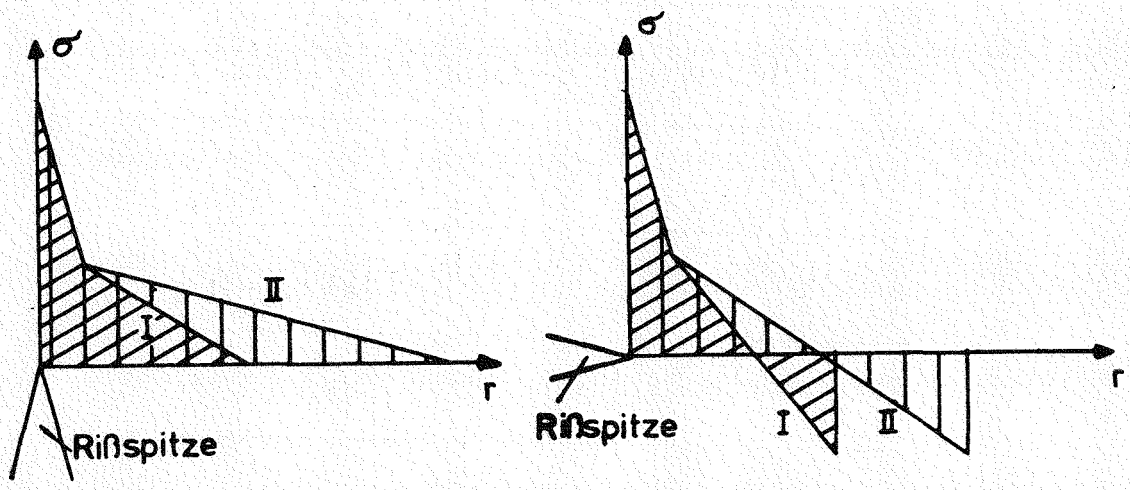

Abb. 33: Schematischer Verlauf der Spannungen mit der Entfernung von der Rißspitze (I: kleine Probe, II: große Probe) a) senkrecht zur Bruchfläche, b) in der Verlängerung der Bruchfläche

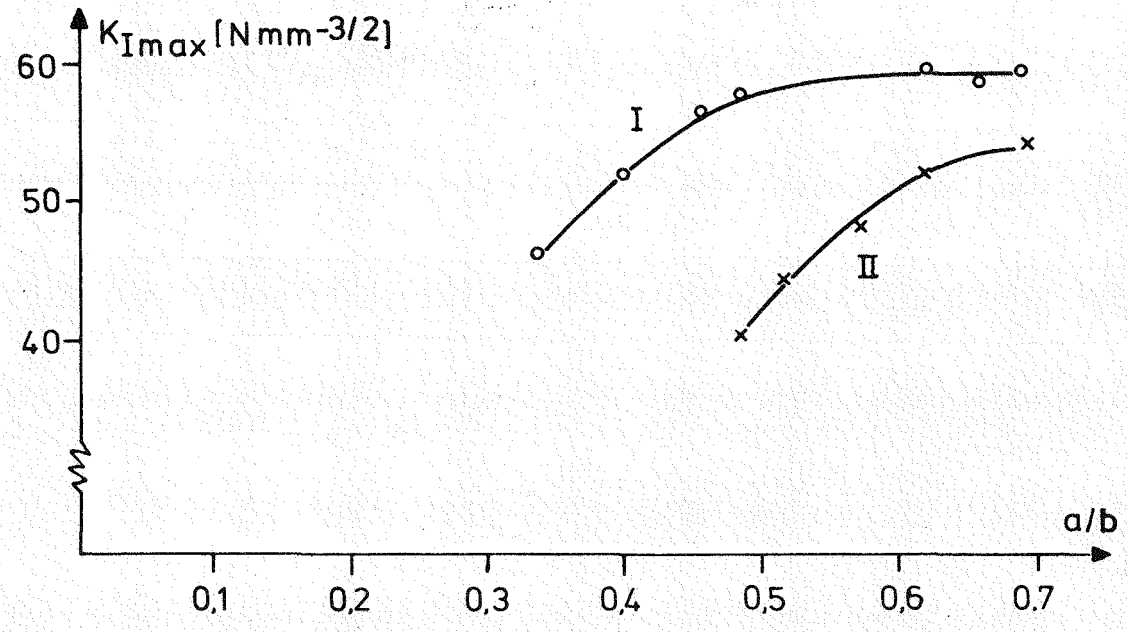

Abb. 34: K_{Imax}-Werte für vorbelastete CT-Proben.
I: kurz, II: tief eingesägte Probe.
Belastungsgeschwindigkeit: 100 µm/min

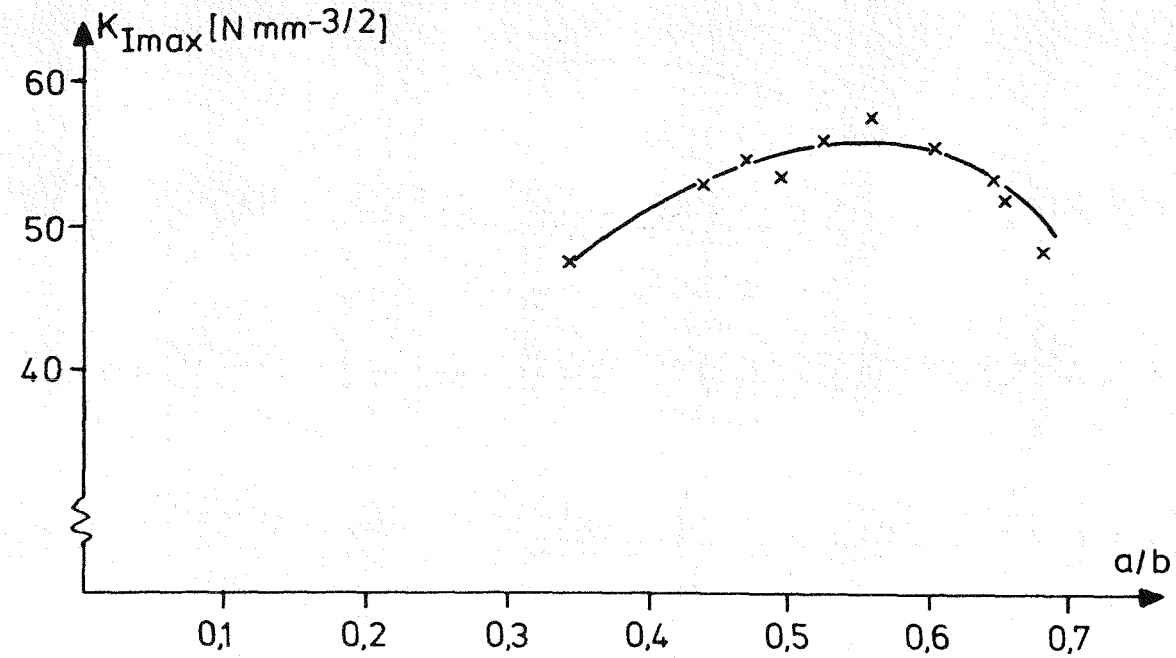

Abb. 35: K_{Imax}-Werte für eine vorbelastete CT-Probe. Belastungsgeschwindigkeit: 25 µm/min

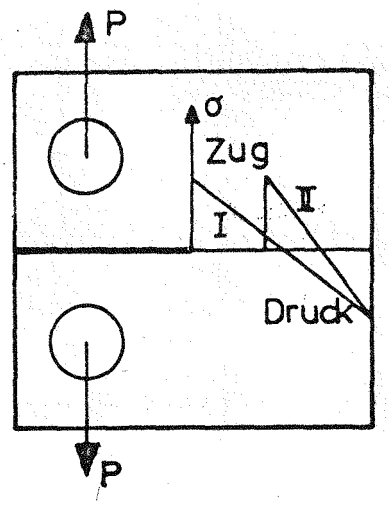

Abb. 36:

Schematischer Verlauf der Zug- und Druckspannungen in der Rißebene einer CT-Probe. I: kurzer Riß, II: langer Riß.

			Elektrode I	Elektrode III
a/b	o,3	K_{Iv} (N/mm$^{-3/2}$)	39,o ± 2,3	35,6 ± 2,o
		K_{Imax} (N/mm$^{-3/2}$)	45,7 ± 2,4	41,3 ± 1,1
a/b	o,7	K_{Iv} (N/mm$^{-3/2}$)	33,3 ± 1,7	28,1 ± 1,5
		K_{Imax} (N/mm$^{-3/2}$)	37,3 ± 1,9	31,8 ± 1,3

Tab. 7: Vergleich der Bruchzähigkeiten identischer Proben aus verschiedenen Elektroden

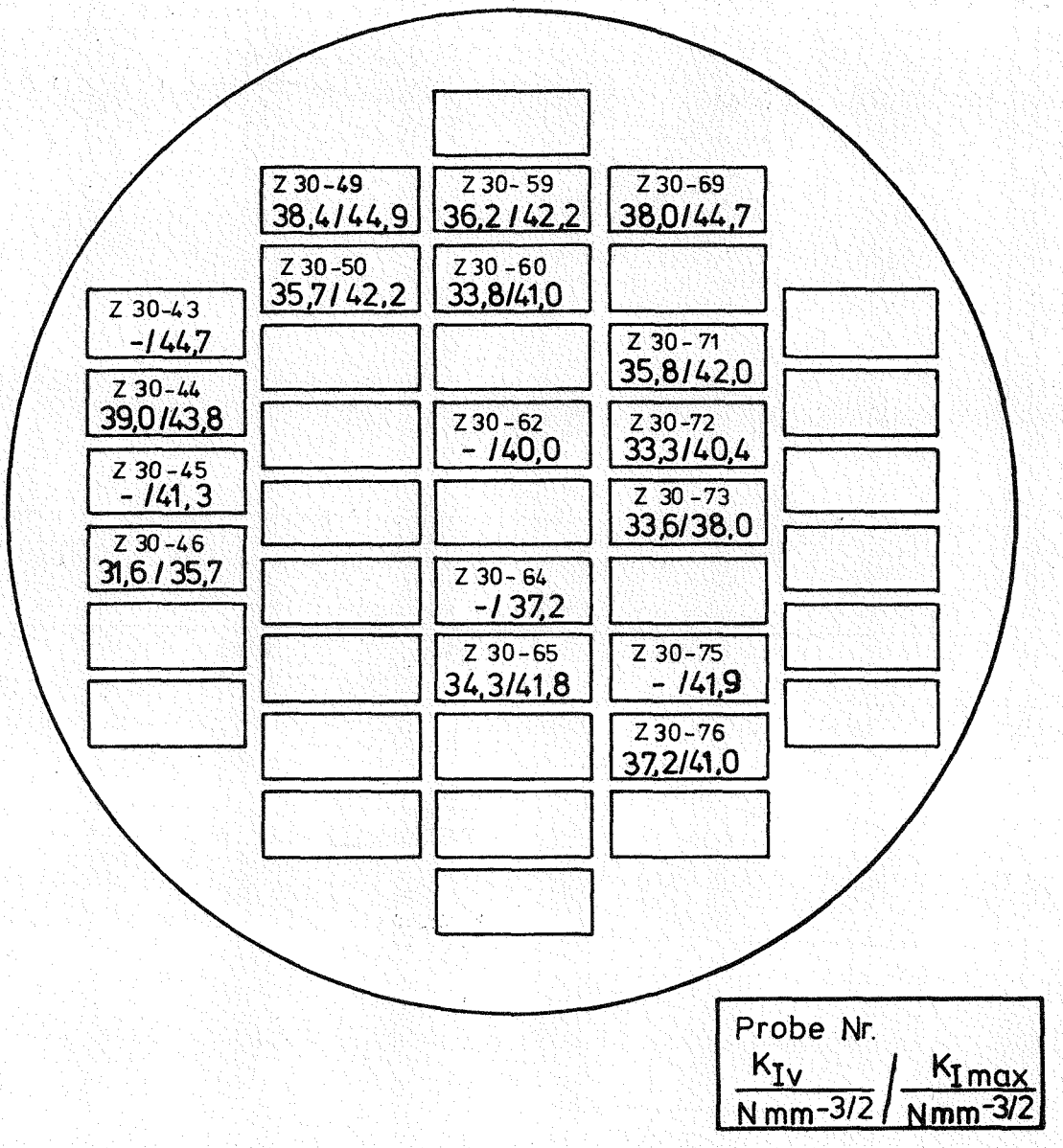

Abb. 37: Entnahmeplan mit Bruchzähigkeiten zu Proben Z 3o, a/b = o,3

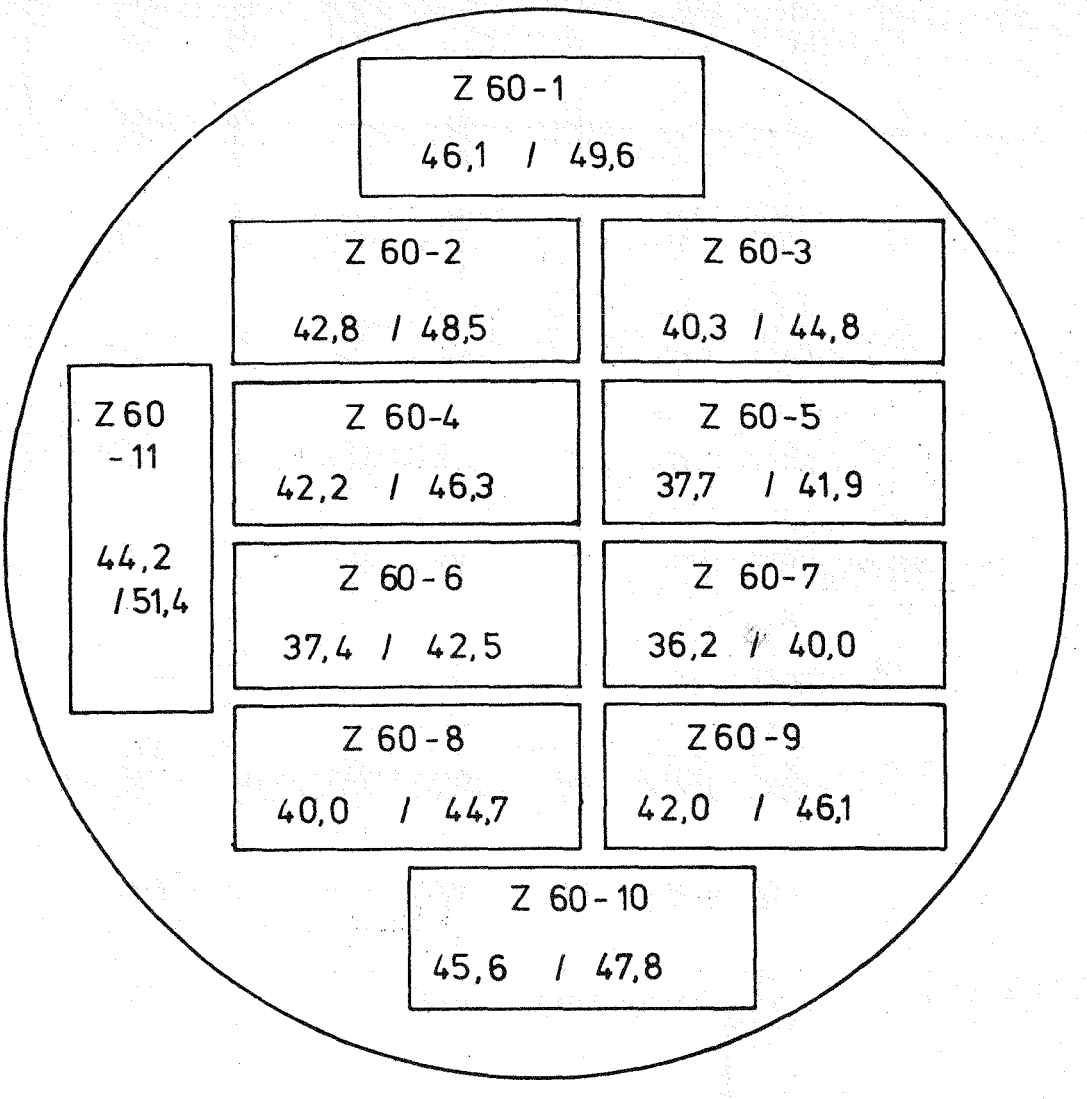

Abb. 38: Entnehmeplan mit Bruchzähigkeiten zu Proben Z 6o, a/b = o,5

	Max. Korngröße (mm)	K_{Iv} ($N/mm^{-3/2}$)	K_{Imax} ($N/mm^{-3/2}$)
AS2-F-5oo	1	35,6 ± 2,o	42,o ± 1,1
AS2-M-5oo	3	33,2 + 1,o	39,7 ± 1,1
AS2-G-5oo	1o	3o,7 ± 4,o	37,6 ± 3,4

Tab. 8: Mittelwerte und Standardabweichungen von Proben aus den Materialien AS2-M-5oo, AS2-M-5oo und AS2-G-5oo

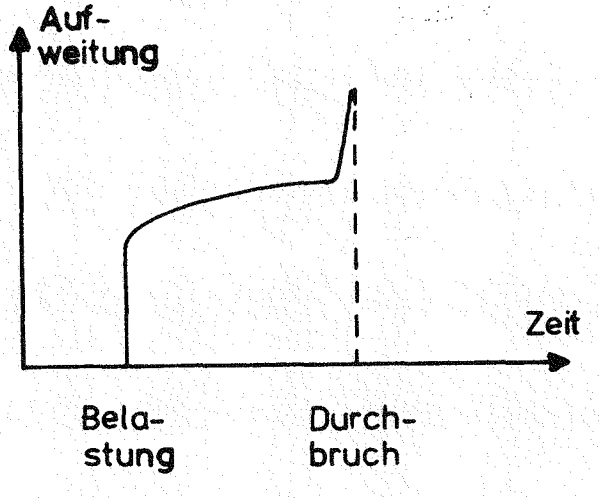

Abb. 39:
Zeitlicher Verlauf der Aufweitung einer CT-Probe unter konstanter Last.

Anhang
======

Benutzte Literatur

1.) Mantell, C.L.: Carbon and Graphite Handbook, New York, 1968

2.) Delle, W.: Über das Bestrahlungsverhalten von Reaktorgraphiten unterschiedlicher Zusammensetzung. KFA-Bericht Jül-747-RW, 1971

3.) Nightingale, R.E.: Nuclear Graphite, New York, 1962

4.) Slagle, C.D.: Journal of the American Ceramic Society 5o (1967) 495

5.) Jenkins, G.M.: Brit. Journal of Applied Physics, 13 (1962) 3o

6.) Förster, F.: Z. Metallkunde, 29 (1937) 1o9

7.) Knott, J.F.: Fundamentals of Fracture Mechanics, London, 1973

8.) Eftis, J. et al.: Basic Concepts in Fracture Mechanics, in H. Liebowitz (Hrsg.): Fracture Mechanics of Aircraft Structures, AGARD No. 176, 1974

9.) Blauel, G.G. et al.: Materialprüfung 12 (197o) 69

1o.) Inglis, C.E.: Proc. Inst. Naval Architects, 55 (1913) 219

11.) Griffith, A.A.: Phil. Trans. Royal Society, Series A, 221 (192o) 163

12.) Smekal, A.: Die Festigkeitseigenschaften spröder Körper, Ergebnisse der exakten Naturwissenschaften, 15 (1936) 1o6

13.) Irwin, G.R.: Fracture, in Handbuch der Physik Band VI, Berlin, 1958

14.) Irwin, G.R.: Journal of Applied Mechanics, 24 (1957) 361

15.) Heckel, K.: Einführung in die Technische Anwendung der Bruchmechanik, München, 197o

16.) Sneddon, I.N.: Proc. Roy. Soc., Ser. A, 187 (1946) 229

17.) Westergaard, H.M.: Trans. ASME, 6 (1939) A-49

18.) Dugdale, D.S.: J. Mech. and Phys. of Solids, 8 (196o) 1oo

19.) Standard Method of Test for Plane Strain Fracture Toughness of Metallic Materials, ASTM E 399-72, in ASTM Book of Standards, Vol. 31, Philadelphia, 1973

2o.) Rooke, D.P., D.J. Cartwright: Stress Intensity Factor Solutions, in H. Liebowitz (Hrsg.): Fracture Toughness Testing of Aircraft Structures, AGARD No. 176, 1974

21.) Brown, W.F., J.E. Srawley: Plane Strain Crack Toughness Testing in High Strength Metallic Materials, ASTM-STP. 41o, Philadelphia, 1966

22.) Link, F., D. Munz: Materialprüfung 13 (1971) 4o7

23.) Dunegan, H.J., A.S. Tetelman: Materialprüfung 14 (1972 153

24.) Corum, J.M.: Journal of Nuclear Materials, 22 (1967) 41

25.) Davidge, R.W., G. Tappin: Journal of Material Science 3 (1968) 165

26.) Slind, L.O.: The Fracture Toughness of Graphite Double Cantilever Beam Specimens, BNWL-CC 774, 197o

27.) Gillis, P.P., J.J. Gilman: Journal of Appl. Physics, 35 (1964) 647

28.) Yahr, G.T., R.S. Valachovic: Proc. of the Conf. on Continuum Aspects of Graphite Design, Gatlinburg/Tenn. 197o

29.) Brocklehurst, J.E., R.G. Brown: Fatigue, Notch Sensitivity and Work of Fracture Studies on Isotropic Graphite, TRG-Report 2513 (S), 1973

3o.) Udovskii, A.L. et al.: Strength of Materials 4 (1972) 595

31.) Vitovec, F.H.: Journal of Testing and Evaluating, 1 (1973) 25o

32.) Steigerwald, E.A., G.L. Hanna: Proc. Am. Soc. Test. Mat. 62 (1962) 885

33.) Marshall, P., E.K. Priddle: Carbon 11 (1973) 541

34.) Buresch, F.E.: pers. Mitteilung

35.) Schmidt, A.: pers. Mitteilung

36.) Seldin, E.J.: Carbon 4 (1966) 177

37.) Cords, H.: pers. Mitteilung

38.) Davies, O.L.: Statistical Methods in Research Production, London, 1961

39.) Blume, J.: Statistische Methoden für Ingenieure und Naturwissenschaftler, Band I, Düsseldorf, 197o